Hindawi
International Journal of Intelligent Systems
Volume 2024, Article ID 7775139, 28 pages
https://doi.org/10.1155/2024/7775139

Research Article

Multiobjective Optimization of Diesel Particulate Filter Regeneration Conditions Based on Machine Learning Combined with Intelligent Algorithms

Yuhua Wang,[1] **Jinlong Li**,[1] **Guiyong Wang**,[1] **Guisheng Chen**,[1] **Qianqiao Shen**,[1] **Boshun Zeng**,[1] **and Shuchao He**[2]

[1]*Yunnan Key Laboratory of the Internal Combustion Engine, Kunming University of Science and Technology, Kunming 650500, China*
[2]*Yunnei Power Co., Ltd., Kunming 650217, China*

Correspondence should be addressed to Guiyong Wang; wangguiyong@kust.edu.cn

Received 20 September 2023; Revised 13 March 2024; Accepted 22 March 2024; Published 1 April 2024

Academic Editor: Vasudevan Rajamohan

To reduce diesel emissions and fuel consumption and improve DPF regeneration performance, a multiobjective optimization method for DPF regeneration conditions, combined with nondominated sorting genetic algorithms (NSGA-III) and a back propagation neural network (BPNN) prediction model, is proposed. In NSGA-III, DPF regeneration temperature (T4 and T5), O_2, NO_x, smoke, and brake-specific fuel consumption (BSFC) are optimized by adjusting the engine injection control parameters. An improved seagull optimization algorithm (ISOA) is proposed to enhance the accuracy of BPNN predictions. The ISOA-BP diesel engine regeneration condition prediction model is established to evaluate fitness. The optimized fuel injection parameters are programmed into the engine's electronic control unit (ECU) for experimental validation through steady-state testing, DPF active regeneration testing, and WHTC transient cycle testing. The results demonstrate that the introduced ISOA algorithm exhibits faster convergence and improved search abilities, effectively addressing calculation accuracy challenges. A comparison between the SOA-BPNN and ISOA-BPNN models shows the superior accuracy of the latter, with reduced errors and improved R^2 values. The optimization method, integrating NSGA-III and ISOA-BPNN, achieves multiobjective calibration for T4 and T5 temperatures. Steady-state testing reveals average increases of 3.14%, 2.07%, and 10.79% in T4, T5, and exhaust oxygen concentrations, while NO_x, smoke, and BSFC exhibit average decreases of 8.68%, 12.07%, and 1.03%. Regeneration experiments affirm the efficiency of the proposed method, with DPF regeneration reaching 88.2% and notable improvements in T4, T5, and oxygen concentrations during WHTC transient testing. This research provides a promising and effective solution for calibrating the regeneration temperature of DPF, thus reducing emissions and fuel consumption of diesel engines while ensuring safe and efficient DPF regeneration.

1. Introduction

With industry development, the energy crises and environmental pollution have been paid more attention [1]. Diesel engine performance optimization and emission control are the main research topics in the diesel engine field [2, 3]. As emissions requirements for diesel engines have become more stringent, different after-treatment technologies have been introduced to the market [4, 5]. DPF is considered one of the most effective after-treatment technologies due to its simple and efficient work. Upon accumulating a designated quantity of particulate matter, the DPF necessitates active regeneration cleaning [6]. The critical aspect of the active regeneration process is maintaining a sufficient interior temperature within the DPF. Optimizing control parameters is essential for reducing diesel fuel consumption and ensuring efficient DPF regeneration.

Previous research has focused on optimizing control parameters, especially in normal engine mode [7]. However, systematic methods to optimize the temperature of DPF

during regeneration are rarely studied. The crucial factor in controlling the regeneration process of the DPF is ensuring that the inlet temperature meets the requirements [8, 9]. During the thermal regeneration process of the DPF, the exhaust temperature at the DPF inlet needs to be heated up to above 500°C to oxidize the accumulated soot particles efficiently. The DPF inlet gas temperature must be accurately controlled to ensure efficient regenerations. Therefore, the combustion parameters of the regeneration mode must be optimized during the development of the diesel electronic control unit (ECU). However, the significant increase in the number of diesel engine control parameters brings tremendous challenges to optimizing diesel engine control parameters. Traditional manual calibration has been unable to meet the demand. Therefore, it is necessary to seek an advanced optimization method to solve the optimization problem of DPF regeneration conditions. This study proposes a multiobjective optimization method for controlling parameters in the diesel engine's DPF regeneration mode.

During DPF regeneration, multiple factors should be considered, such as DOC and DPF inlet temperatures, smoke, NO_x, O_2 concentrations, and fuel consumption. Therefore, it is necessary to introduce a multiobjective optimization method to seek the "balance point" among multiple objectives. Optimizing the control parameters to achieve the optimal regeneration temperature of the DPF is a multiobjective optimization problem. Various optimization methods, including multiobjective PSO [10], NSGA-II [11], GA [12], and hybrid approaches [13], have been employed in studies to enhance the performance of internal combustion engines. These methods focus on optimizing critical parameters to achieve improvements in emissions, fuel consumption, and overall efficiency. This is important for controlling the DPF regeneration process.

However, all previous studies need to formulate a new single-objective optimization problem to deal with the multiobjective optimization problem [14]. The optimization problem of diesel engine operating parameters is characterized by high dimensionality, nonlinearity, uncertainty, and noise interference [15]. These factors can lead to low accuracy and slow convergence of optimization algorithms. NSGA-III is an improved algorithm based on NSGA-II, which can ensure the calculation speed and make the results closer to the theoretical optimal value [16]. In multiobjective optimization, multiple operating conditions of the diesel engine need to be evaluated, and the parameter search needs to be performed to determine the impact on engine performance [7]. The assessment of these operating conditions is impractical through engine bench tests alone. Therefore, many predictive models have been developed for engine research and optimization.

In recent years, model-based virtual calibration technology has been widely studied in the diesel engine field. At present, the mathematical model of the diesel engine can be divided into the volume method [17, 18], the average value method [19, 20], and the machine learning algorithm method [21]. It is challenging to describe the diesel engine with simple data formulas and physical models [22, 23]. Traditional diesel engine modeling makes it difficult to satisfy the requirements for prediction accuracy and real-time. Machine learning has become increasingly popular in recent years [24]. Kin et al. [25], Francesco et al. [26], Kumar et al. [27], and Ağbulut et al. [28] have demonstrated that machine learning models exhibit higher prediction accuracy, reduced calibration time, and increased efficiency in predicting diesel engine performance. However, the ANN may converge to the local minimum and face the problem of overfitting after training with a large amount of data [29]. GA [30], ant colony algorithms [31], and simulated annealing algorithms [32] are often used to optimize the model parameter. Experiments are conducted to verify the validity of the optimized parameters. However, these optimization algorithms have problems such as low theoretical complexity, slow model prediction speed, and premature convergence. Therefore, this study aims to improve the optimization algorithm. The complex DPF regeneration temperature calibration involves multiple control parameters and response values. Using machine learning for prediction models can enhance the efficiency of optimization, reducing calibration costs while ensuring the accuracy of the results.

Thus, this study needs to address the following: (1) ensure that the DPF efficiently removes accumulated particles during the regeneration process, maintaining its normal functionality and reducing particulate emissions from diesel engines, (2) optimize multiple control parameters during DPF regeneration mode to balance objectives such as DOC inlet temperature, DPF inlet temperature, emission concentration, economy, and fuel consumption, (3) enhance accuracy and efficiency in diesel engine regeneration mode to avoid issues such as overfitting in ANN, and (4) choose an appropriate multiobjective optimization algorithm to address challenges in optimizing control parameters for diesel engines, considering high dimensionality, nonlinearity, uncertainty, and noise interference.

Therefore, a multiobjective optimization method of DPF regeneration condition based on NSGA-III coupled with ISOA-BP was proposed. The aim is to optimize the regeneration conditions of the DPF, ensuring safe and efficient regeneration while minimizing diesel engine emissions and fuel consumption. Based on the experimental data, the performance prediction model of BPNN in diesel engine regeneration mode was established. The SOA algorithm is introduced to optimize the initial weight and threshold of BPNN. In addition, to ensure the precision of both the BPNN model and optimization outcomes, a novel enhancement algorithm, ISOA, is introduced to optimize the initial parameters of BPNN. ISOA is employed to optimize the model structure parameters, ensuring that the model's predictive accuracy aligns with the optimization criteria. The optimization objectives during diesel particulate filter (DPF) regeneration include DOC inlet temperature, DPF inlet temperature, exhaust oxygen concentration, economy, and emissions. Then, combined with the optimization model of NSGA-III for multiobjective optimization, the optimal injection parameters are obtained. ISOA-BP is used to evaluate the fitness of the Pareto optimal solution. The optimal control parameters are determined from the Pareto optimal

solution set by dynamically adjusting the weights. Finally, three experimental methods are employed to validate the obtained results.

The research novelty of the proposed work is described as follows: (1) a multiobjective optimization method for DPF regeneration condition is proposed. Integrating NSGA-III with a BPNN prediction model enables simultaneous optimization of multiple parameters including DPF regeneration temperature, O_2, NO_x, smoke, and BSFC, leading to comprehensive improvements in emissions and fuel consumption, (2) based on the SOA optimization algorithm, the ISOA algorithm is proposed, which can quickly converge and find the global optimal solution, and (3) the use of an ISOA enhances the accuracy of the BPNN prediction model, resulting in a more precise evaluation of fitness for optimized fuel injection parameters.

2. Experimental Design and Methods

2.1. Experimental Design for DPF Predictive Modeling. The optimization of DPF regeneration conditions includes the calibration of DOC inlet temperature (T4) and DPF inlet temperature (T5). A simplified schematic of T4 and T5 is shown in Figure 1. DOC inlet temperature calibration is to raise the diesel engine exhaust temperature by adjusting the fuel system control parameters and the intake system control parameters. The aim is to bring the DOC up to the starting ignition temperature. The DPF inlet temperature increase mainly depends on the diesel secondary injection to provide additional HC. The DOC raises the DPF inlet temperature by oxidative warming to ensure a high enough temperature inside the carrier during DPF regeneration.

During the regeneration of the DPF, the goal of T4 optimization is to attain a temperature of 200°C. This temperature is crucial to ensure the effective oxidation of the DOC. The objective of T5 optimization is to supply a suitable quantity of HC for DOC oxidation heating, which will lead to increased temperature of T5 and ensure efficient and safe regeneration of DPF.

In order to optimize the DPF regeneration conditions, a total of eight control parameters were selected for calibration: preinjection timing, preinjection fuel quantity, main injection timing, rear injection 2 timing, rear injection 2 fuel quantity, rear injection 1 fuel quantity, intake volume demand value, and rail pressure. According to the initial control MAP in the regeneration mode of the diesel engine, the range settings of the eight control parameters in the selected speed interval are shown in Table 1. The optimal control parameters for extreme conditions at the edge of the diesel section may be outside the setting range in Table 1. In order to make the DPF regeneration condition prediction model accurately predict the diesel engine's performance near the marginal operating conditions, the preinjection timing, main injection timing, and rear injection 2 timing were increased by 2~3°CA. The rear injection 2 and rear injection 1 fuel ranges were appropriately increased by 1~2 mg/cycle during the test design. T4, T5, O_2, BSFC, NO_x, turbine front-end temperature, and smoke data were collected for the experiment.

To construct the DPF regeneration temperature prediction model, sample data of injection control parameters corresponding to T4, T5, O_2, BSFC, NO_x, turbine inlet temperature, and smoke are essential for model learning and training. The diesel engine experiments were conducted in regeneration mode. Due to the addition of two rear injections, the exhaust temperature will be higher than the normal mode. In the experiment, the diesel engine speed range of 1000 r/min~2800 r/min and torque range of 0~400 Nm were selected for DPF regeneration temperature calibration. To facilitate the experimental design, the speed and torque are selected as the operating parameters. The diesel engine torque should be limited to the external characteristic range. The external characteristic curve in the selected speed range of the diesel engine is shown in Figure 2.

A total of 10 characteristic values are involved in the design of the space-filling test. The rail pressure is not applied in the space-filling test design but is obtained through the bench monitoring system. The experimental design of nine characteristic control parameters was completed by the Sobol space-filling method. At the same time, 10 operating points were set for each speed and torque, and 100 simple test design points were added. Experiments were performed from small to large in turn according to torque at each speed. Other eight characteristic values and each output response value were recorded to improve and verify the model's accuracy. A total of 720 test points in the test program were used to construct the DPF regeneration performance prediction model. To ensure the accuracy of the test results, each test point must be repeated three times, and the final results are taken as the average of the three tests. The design points of the Sobol sequence space-filling experiment are shown in Figure 3.

2.2. Experimental Equipment. A four-cylinder diesel engine was used in the experiment. Tables 2 and 3 show the parameters of the engine, dynamometer, and related instruments. Eddy current dynamometer and related instruments were used to measure the speed and torque of the engine in the experiment; engine fuel temperature and pressure, coolant temperature, intake temperature and pressure, exhaust pressure, atmospheric humidity, temperature, and pressure were measured by the engine state parameter tester. The altitude of the diesel engine bench test environment is 2000 m. The temperature of the test environment is 25°C, atmospheric pressure is 80 kPa, atmospheric humidity is about 50%, fuel temperature is maintained at 30°C, oil temperature is controlled at about 90°C, and cooling water temperature is about 90°C. The diagram of the diesel engine bench is shown in Figure 4. The physical diagram of the diesel engine bench equipment is shown in Figure 5. Table 4 shows some experimental data.

2.3. Uncertainty Analysis. All experimental measurements are subject to some error or uncertainty. The uncertainty in the experimental results will arise from the condition, calibration, sensor selection, test procedure, and observation. Uncertainty analysis calculations can improve the accuracy

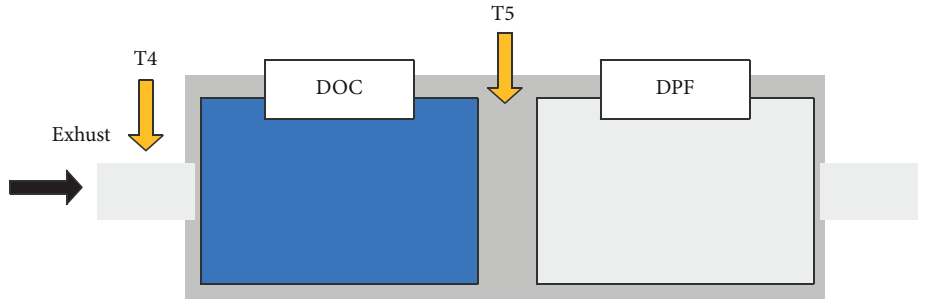

Figure 1: Simplified diagram of T4 and T5.

Table 1: Control parameter range setting.

Control parameter	Range (unit)
Preinjection timing	3~45 (°CA)
Main injection timing	−10~15 (°CA)
Rear injection 2 timing	−48~−14 (°CA)
Preinjected fuel quantity	1.5~2 (mg/cyc)
Rear injection 2 fuel quantity	0~9.5 (mg/cyc)
Rear injection 1 quantity	0–9 (mg/cyc)
Rail pressure	38~182 (MPa)
Intake volume	400~1600 (mg/cyc)

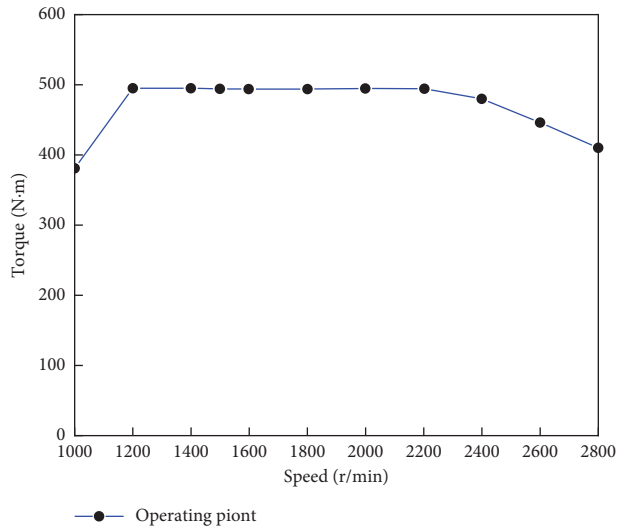

Figure 2: The full-load lug curve of the diesel engine.

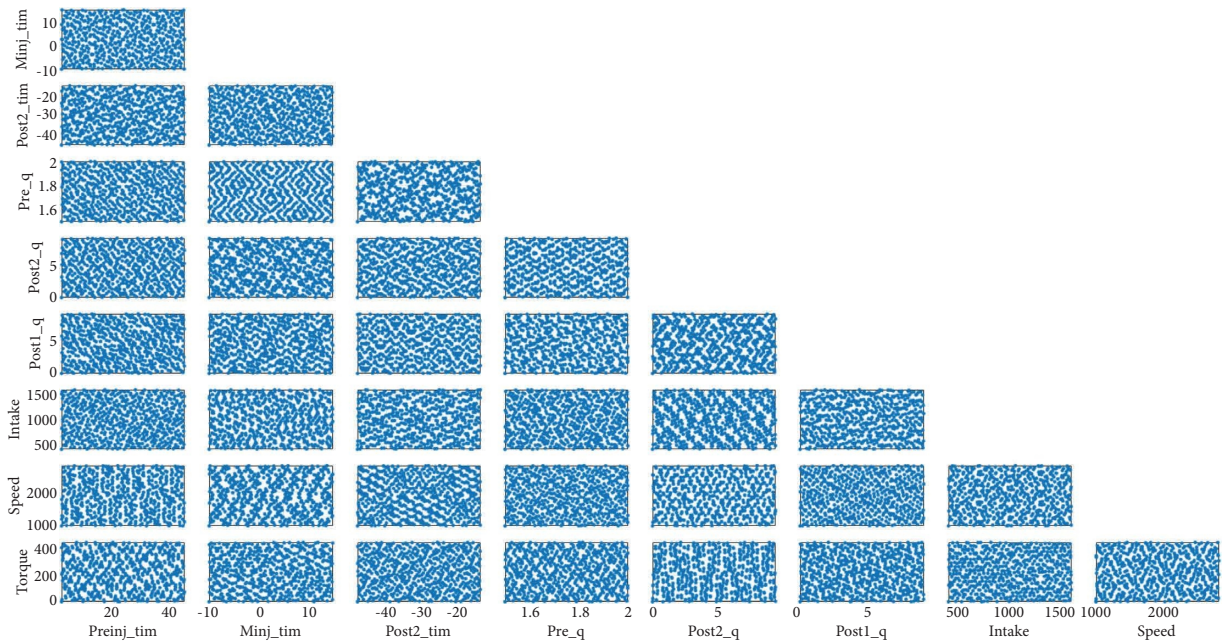

Figure 3: Space-filling test design point.

Table 2: Basic parameters of D25TCI diesel engine.

Parameter	Value
Cylinder diameter (mm)	92
Stroke (mm)	94
Displacement (L)	2.5
Rated power (kW)	120
Rated speed (r/min)	3600
Maximum torque (N·m)	400
Maximum torque speed (r/min)	1600–2800
Maximum burst pressure in the cylinder (bar)	160
Compression ratio	17.5

Table 3: Specific model of test equipment.

Equipment	Specification
Coolant control system	FEV CoolCon LS
Fuel control system	FEV FuelCon
Fuel consumption meter	FEV FuelRate
Oil conditioning system	FEV LubConLS
Pressurized intercooling temperature control system	FEV CoolSIM
Signal acquisition box	FEV InterRate
Dynamometer	Dyna craft 250HS
Measurement and control system	TOM/TCM/TEM
Emission analyzer	MEXA-7500DEGR
Smoke meter	AVL 415
Mass flowmeter	Sensyflow
Exhaust back pressure control system	FEV ExCon LS
Calibration interface module	ETAS ES592

of experimental measurement data, which is crucial for improving diesel engine prediction models. The uncertainty percentage can be calculated by using the following equation:

$$E_R = \left\{ \left[\left(\frac{\partial R_a}{\partial L_1} \right) u_1 \right]^2 + \left[\left(\frac{\partial R_a}{\partial L_2} \right) u_2 \right]^2 + \cdots + \left[\left(\frac{\partial R_n}{\partial L_n} \right) u_n \right]^2 \right\}^{1/2}, \quad (1)$$

$$R_a = \{L_1, L_2, L_3, \cdots L_n\}, \quad (2)$$

where R_a is the independent variable function of $L_1, L_2, L_3, \ldots,$ and L_n and $u_1, u_2, \ldots,$ and u_n are the independent variable uncertainties, respectively.

The overall uncertainty in the experimental procedure can be derived from the following equation.

Thus, the overall experimental uncertainty T_E is

$$T_E = \sqrt{\begin{matrix} E_{R(T4)}^2 + E_{R(T5)}^2 + E_{R(\text{Smoke})}^2 + E_{R(\text{Oxygen})}^2 \\ + E_{R(\text{NOx})}^2 + E_{R(\text{BSFC})}^2 + E_{R(\text{Temperature})}^2 \end{matrix}} = 2.53\%. \quad (3)$$

3. Prediction Model

3.1. BPNN Model. BPNN is commonly utilized for supervised training, given the random initialization of network weights and biases during the initial phase. The DPF performance prediction model of the diesel engine has 10 characteristic inputs and 7 response outputs. The prediction model topology is shown in Figure 6.

The normalization formula of sample data is as follows:

$$y = \frac{x - x_{\min}}{x_{\max} - x_{\min}}, \quad (4)$$

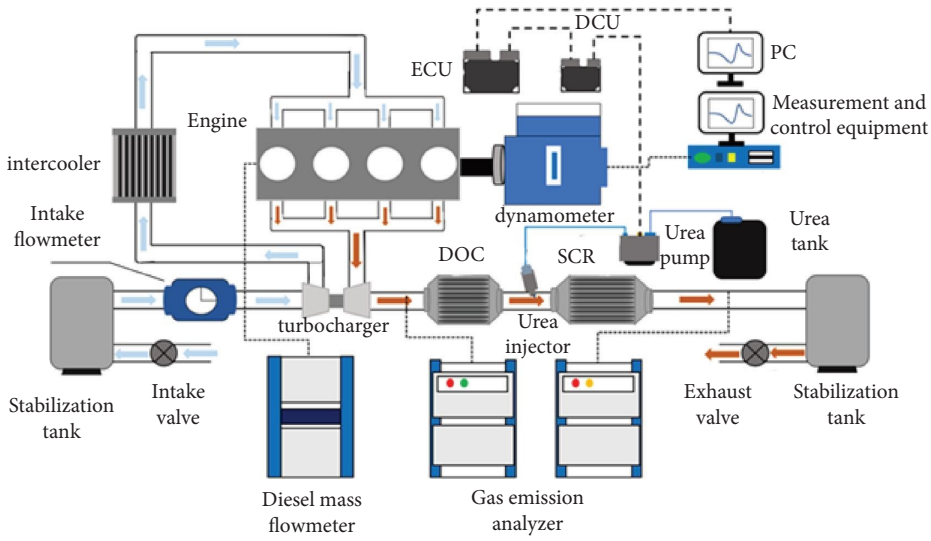

Figure 4: Diesel engine bench structure.

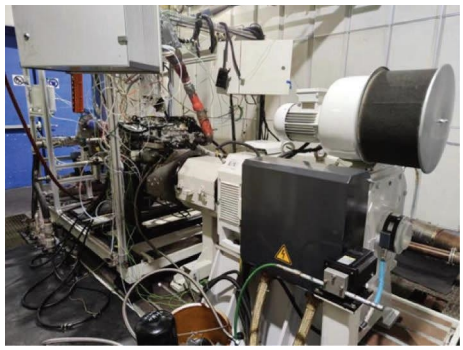

Figure 5: Test equipment of the engine bench.

Table 4: Partial experimental data.

	Speed (r/min)	Torque (Nm)	Preinjection quantity (mg)	Rear injection 1 quantity (mg)	Rear injection 2 quantity (mg)	Rear injection 2 timing (°CA)	Main injection timing (°CA)	Preinjection timing (°CA)	Intake demand (mg/cyc)	T4 (°C)	T5 (°C)
1	1000	20	1.66	7.26	2	−33.19	0.044	11.426	681	308.16	502.86
2	1400	180	1.84	4.10	0.00	0.00	10.50	39.13	1409.0	514.66	600.06
3	1600	360	1.60	3.20	2.50	−33.00	−4.00	8.50	980.0	415.26	488.66
4	1800	20	1.60	8.00	5.00	−29.99	−2.00	11.01	650.0	305.76	598.86
...	...	...									
597	2800	45	1.88	3.16	8.76	−40.30	1.69	15.97	775.0	485.06	582.86
598	2600	270	2.10	4.30	3.00	−29.99	9.01	28.02	1440.0	510.66	608.26
599	2400	225	1.84	5.70	2.10	−26.77	10.00	34.30	1520.0	492.06	607.26
600	2800	360	1.86	3.98	5.20	−29.99	6.00	20.81	522.0	406.46	609.26

where x and y are the sample values before and after normalization and $x_{\min}$ and $x_{\max}$ are the maximum and minimum values of samples, respectively. The neuron node input is $x = [x_0, x_1, x_2, \ldots, x_n]$, where each input node and the node corresponding weights are $w = [w_{i0}, w_{i1}, w_{i2}, \ldots, w_{\text{in}}]$. In the forward propagation process, the input of each node is summed by a weighted sum and then calculated by an activation function to get the corresponding output. The mathematical description of the process is as follows:

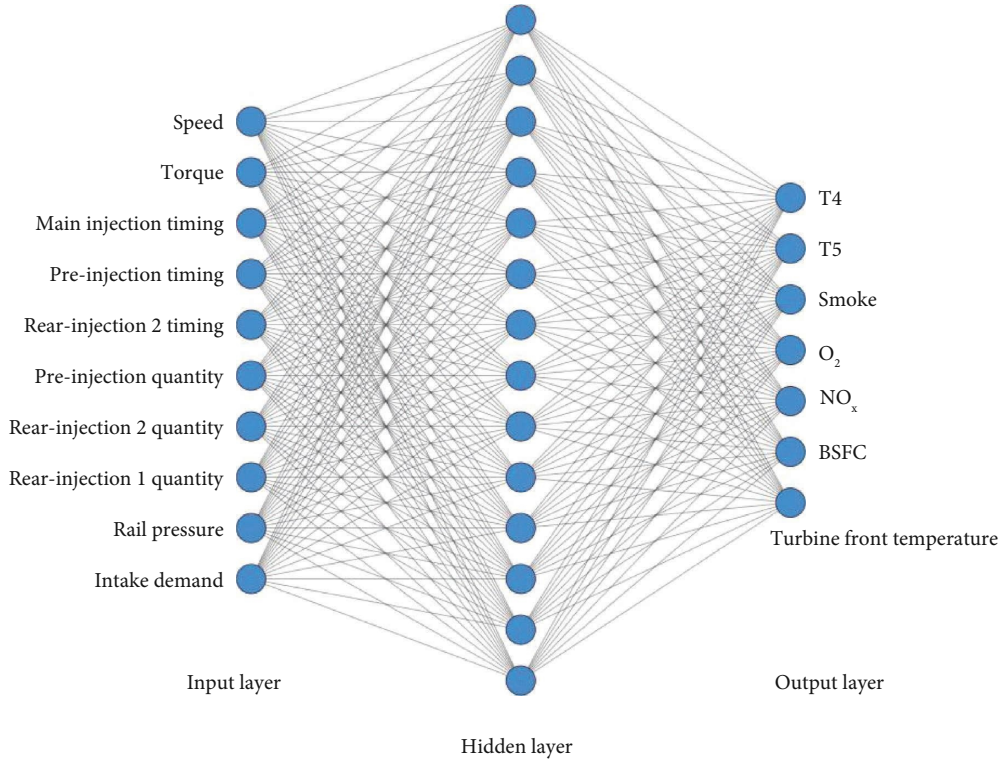

Figure 6: Prediction model topology.

$$\text{net}_i = \sum_{j-1}^{n} w_{\text{ij}} x_j - \theta + \text{b}_i = \text{xw} + b_i, \tag{5}$$

$$y_i = f(\text{net}_i) = f(\text{xw} + b_i), \tag{6}$$

where when $x_0 = -1$, w_{i0} is θ; b_i is the threshold value at the ith neuron node; $f(*)$ is the activation function; and y_i is the output value of this neuron node.

The training error of BPNN is a function of the difference between the expected output and the actual output and the model error formula is

$$E_p = \frac{1}{2} \sum_{j-1}^{n} (t_i - y_i)^2, \tag{7}$$

where t_i is the expected output value of the ith neuron node and y_i is the actual output value of the ith neuron node. The learning rate given for error E_p is η, and the range of η is (0, 1).

BPNN constantly improves the model's accuracy through forward propagation and reverse transmission of error correction weights and thresholds, which is the model's training process. When the model accuracy reaches the requirement, or the algorithm reaches the maximum number of iterations, the algorithm terminates the iteration and outputs the final result. The details about the ANN theory can be found in [33, 34].

3.2. SOA Optimization and Improvement. BPNN has the problem of overfitting and falling into local optimal solutions, which leads to low prediction accuracy. In order to improve the training speed and prediction accuracy of the prediction model and ensure the accuracy of DPF regeneration temperature calibration, the BPNN optimization can improve the prediction accuracy. SOA is introduced to solve the above problems, improve the SOA, and propose ISOA. ISOA optimizes the initial weights and thresholds of BPNN. ISOA optimizes the initial weights and thresholds of BPNN.

3.2.1. SOA. The SOA is a new swarm intelligence algorithm proposed by Gaurav Dhiman according to seagull's migration and predation rules. SOA has the advantages of simple structure, fast convergence, and high optimization precision. The gull algorithm can be divided into migration (global search) and predation (local search).

(1) Migration Process (Global Search). During migration, seagulls must avoid collisions between each individual so that each population renewal does not produce duplicate individuals. The convergence factor A is used to control the position update of each individual. The position update formula is as follows:

$$C_s(t) = A \times P_s(t), \tag{8}$$

where $C_s(t)$ is the position that does not conflict with other individuals, $P_s(t)$ is the current position of an individual seagull, and t is the number of iterations.

The convergence factor A describes the movement of a seagull in the solution space and the expression is

$$\mathrm{A} = f_c \times \left(1 - \frac{t}{T}\right), \tag{9}$$

where T is the maximum number of iterations and f_c is the control factor, and its value is usually set to 2. Seagull individuals will move towards the optimal individual after updating their position. The direction the seagull moves toward the optimal individual is represented as

$$M_s(\mathrm{t}) = B \times \left[P_{\mathrm{bs}}(t) - P_s(t)\right], \tag{10}$$

where $P_{\mathrm{bs}}(t)$ is the position of the current optimal individual, $M_s(t)$ is the relative direction between the seagull individual and the optimal individual, and B is the variable that balances global search and local search, and the expression is

$$B = 2 \times A^2 \times R, \tag{11}$$

where R is the random number in [0, 1]. Individual seagulls are constantly moving and arrive at a new location before the global search is over.

$$D_S(t) = \left| C_S(t) + M_S(t) \right|. \tag{12}$$

(2) Predation Process (Local Search). Seagulls attack when they get close to their prey (optimal individuals). A seagull in the air will fly in a spiral trajectory toward its prey and constantly change speed and angle. The mathematical description of this process is as follows:

$$\begin{aligned} x &= r \times \cos(\theta) \\ x &= r \times \sin(\theta) \\ z &= r \times \theta \\ r &= u \times e^{\theta v}, \end{aligned} \tag{13}$$

where r is the spiral radius, θ is the random number in [0, 2π], and u and v are spiral shape parameters. Seagulls hover down in the air and eventually reach their prey.

$$P(t) = D_s(t) \times x \times y \times z + P_{\mathrm{bs}}(t). \tag{14}$$

3.2.2. Algorithm Improvement. The initial population of seagulls is randomly generated in the solution space, and it is impossible to control that each generated population is evenly distributed throughout the solution space. When the algorithm falls into the local optimal, there is no operation out of the local optimal, and the final output result is not globally optimal. If the algorithm cannot find the global optimal solution, the optimal connection weights and thresholds of the BPNN cannot be found. There is a significant error in predicting the DPF regeneration performance parameters of the diesel engine. Thus, ISOA is proposed to address the abovementioned issues.

When the initial population is not uniformly distributed, it can lead the algorithm to a local optimum. Chaotic mapping is widely used in optimization because of its randomness and global stability. Chaotic mapping can replace random number generators to generate chaotic sequences to initialize the population with good results. The tent map is one of the most common chaotic maps. It has a uniform distribution function and good correlation. It can generate an evenly distributed population at population initialization. Its expression is as follows:

$$x_{k+1} = \begin{cases} \dfrac{x_k}{a}, & x_k \in [0, a), \\ \dfrac{(1 - x_k)}{(1 - a)}, & x_k \in [a, 1], \end{cases} \tag{15}$$

where x_k is the chaos value generated by the kth iteration and a is the random number in [0, 1].

The distribution of 1000 chaos values generated by the tent chaos mapping in the interval [0, 1] is shown in Figure 7. The chaos value is generated iteratively according to the mapping formula. When a and k are constant, the chaos number generated each time is the same and can be evenly distributed in the whole solution space. Therefore, chaotic mapping initialization can effectively avoid the problem of SOA's uneven initial population distribution.

In order to achieve sufficient global search and local search in the iterative process, the hyperbolic tangent function is introduced, and the convergence factor A is treated nonlinearly. The hyperbolic tangent function $\tanh(x)$ can be expressed as

$$\tanh(x) = \frac{e^x - e^{-x}}{e^x + e^{-x}}. \tag{16}$$

The $\tanh(x)$ function is stretched, symmetric, and shifted over the interval [−3, 3], and by substituting formula (6) into it, we get

$$A = \tanh\left(\frac{3}{2} f_c - 3 f_c \cdot \frac{t}{T}\right) + 1. \tag{17}$$

The comparison of the convergence factor A before and after the improvement is shown in Figure 8. The value of A decreases slowly in the first iteration, which is conducive to increasing the search range of the seagull in the solution space. A fast decline can accelerate algorithm convergence in the middle stage of iteration. In the late iteration period, the value of A is small and changes slowly, increasing the algorithm's searchability in the local scope.

When the fitness value of the seagull individual is smaller than the population, to enhance the algorithm's optimization ability in the late iteration period, adaptive inertia weight is introduced to balance the global search and local search. The inertia weight formula is as follows:

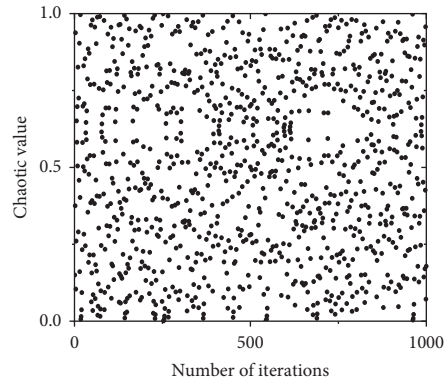

Figure 7: Tent chaotic map distribution.

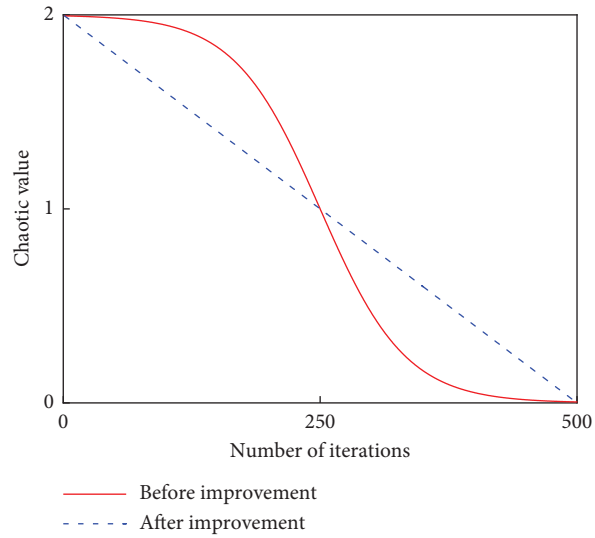

Figure 8: Comparison of convergence factors before and after improvement.

$$\omega(t)_i = \omega_2 + \frac{\omega_2 - \omega_1}{T} \cdot \frac{f(t)_i - f(t)_{\text{avg}}}{f(t)_{\max} - f(t)_{\min}}, \quad f(t)_i < f(t)_{\text{avg}}, \tag{18}$$

where $\omega(t)_i$ is the weight of the ith seagull individual in the t search, ω_1 and ω_2 are the initial minimum and maximum weights, and $f(t)_{\text{avg}}$, $f(t)_{\max}$, and $f(t)_{\min}$ are the mean value, maximum value, and minimum value of population fitness in the t-th iteration.

After introducing adaptive inertia weight, the expression of variable B is

$$B = 2 \times \omega(t)_i \times A^2 \times R. \tag{19}$$

Cauchy variation can increase population diversity and accelerate the movement of seagulls toward the global optimal solution. Gaussian variation can enhance the local search ability of the algorithm to avoid getting into a local optimum dilemma and strengthen the ability of the algorithm to jump out of the local optimum. The equations of Cauchy variation and Gaussian variation are as follows:

$$\begin{aligned} P_s(t) &= P_s(t) + P_s(t) \times \text{Cauchyrd} \\ P_s(t) &= P_s(t) + P_s(t) \times \text{Gaussianrd}, \end{aligned} \tag{20}$$

where Cauchyrd is a random number obeying Cauchy distribution and Gaussianrd is a random number conforming to Gaussian distribution.

The optimal fitness change rate of the population was introduced to determine when the algorithm carried out Gaussian variation. When the rate of change of the optimal fitness of the gull population is less than a threshold α for n consecutive generations, the algorithm performs a Gaussian variation. The decision formula is

$$\left| \frac{f(P_{\text{bs}}(t)) - f(P_{\text{bs}}(t-n))}{f(P_{\text{bs}}(t))} \right| \le \alpha, \quad t > n, \tag{21}$$

where $f(P_{\text{bs}}(t))$ is the optimal fitness value of the seagull population, $n = 10$, and the threshold α is 0.0001.

3.2.3. Performance Comparison before and after Algorithm Improvement. In order to verify the ISOA performance, the SOA and ISOA were compared with different single-peak test functions and multipeak test functions. The single-peak test has only one strict, extreme point in the solution space, which can effectively test the global search ability of the algorithm. The multimodal test function encompasses multiple extreme points within the defined solution space. This characteristic allows for a more comprehensive evaluation of the algorithm's convergence rate and calculation accuracy while also serving to assess whether the algorithm is susceptible to local optima. The algorithm test function is shown in Table 5. TF1–TF4 is a single-peak test function and TF5–TF8 is a multipeak test function.

The convergence curves of SOA and ISOA under 8 test functions are compared, as shown in Figure 9. ISOA can converge to the optimal value faster in the calculation process. The calculation accuracy of ISOA is higher. ISOA requires fewer iterations than SOA when the computational results are the same. In the TF8, the optimal fitness value of ISOA is able to stop and hold around the theoretical optimal value. However, the optimal fitness value of SOA exhibits rapid fluctuations without converging near the theoretical optimum. The algorithm persists in iterative processes, potentially converging into a local optimum. Thus, the ISOA algorithm exhibits superior global and local search capabilities during computation. The ISOA enhances global search and local search capabilities, speeds up the algorithm's convergence, and adds the operation of jumping out of the local optimum to the algorithm.

3.3. Model Evaluation

3.3.1. Model Evaluation Index. The predictive ability of the training model is verified by using the test set in the model performance evaluation. The mean absolute error (MAE), root mean square error (RMSE), mean absolute percentage error, and fitting coefficient (R^2) are used to evaluate the model's accuracy. The calculation formula for each evaluation index is

$$\begin{aligned} \mathrm{MAE} &= \frac{1}{n}\sum_{i=1}^{n} |x_i - x| \\ \mathrm{RMSE} &= \sqrt{\frac{1}{n}\sum_{i=1}^{n}(x_i - x)^2} \\ \mathrm{MAPE} &= \frac{1}{n}\sum_{i=1}^{n}\frac{|x - x_i|}{x} \times 100\%, \\ R^2 &= 1 - \frac{\sum_{i=1}^{n}(x_i - x)}{\sum_{i=1}^{n}(x_i - \bar{x})}, \end{aligned} \tag{22}$$

where n is the number of samples and $x_i, x, \bar{x}$ are, respectively, the predicted values, test values, and average values of the 7 parameters including T4 temperature, T5 temperature, original smoke emission, O_2 concentration, NO_x, BSFC, and turbine inlet temperature.

3.3.2. Model Evaluation. SOA is applied to optimize the initial weights and thresholds of the BP neural network prediction model, aiming to enhance the accuracy of the DPF regeneration condition prediction model. SOA and ISOA optimized the initial weight and threshold of BPNN, respectively, and the prediction accuracy of both models was compared. The algorithm population was set to 50, and the maximum number of iterations was set to 500. The fitness function is the test set's average RMSE of T4 temperature, T5 temperature, O_2 concentration, NO_x, smoke, BSFC, and turbine inlet temperature parameters. The specific steps are shown in Figure 10:

In order to avoid the contingency of model prediction results, the K-fold cross-validation method was used to verify the model. A total of 720 data samples were used to train and verify the model. The ratio of the training set to the test set of the model is 9 : 1. The K-fold cross-validation is selected as the model validation method. The prediction accuracy of SOA-BP and ISOA-BP models was compared and analyzed. The performance of the two models in predicting T4, T5, O_2, NO_x, smoke, BSFC, and turbine inlet temperature is compared in Figure 11.

The X-axis and Y-axis represent the experimental data and predicted values, respectively. R^2 represents the fitting degree of the model. The closer the R^2 value is to 1, the closer the output value of the prediction model is to the experimental target value. The higher the R^2, the higher the model's prediction accuracy and generalization ability. Both models accurately predict T4, T5, smoke, O_2 concentration, NO_x, and BSFC. However, the BPNN model still has large errors in predicting O_2 and smoke even after SOA optimization. R^2 of the model before improvement is 0.94 in predicting both O_2 concentration and smoke. Although the linear fitting and A = P are very close, the whole line presents a parallel state. Therefore, the model can predict the trend of O_2 concentration and smoke intensity. However, the prediction accuracy is insufficient, and the linear fitting degree is slightly poor. The model's MAPE for smoke prediction is 61.43%. Most predicted values are distributed on both sides of the linear fitting line, and the linear fitting line has deviated from line A = P. The irregularity in the sample data and the presence of noise points pose challenges to the model's training, contributing to the suboptimal smoke prediction performance. Due to the small order of magnitude of smoke, the smoke value is below 0.1 FSN in many operating conditions. Even though the model's predicted value is close to the test value, there is a large gap of orders of magnitude between the two values, resulting in a large final error.

However, the ISOA-BPNN model can solve the problem of low accuracy in O_2 and smoke degree prediction. Meanwhile, the prediction accuracy of other parameters is improved. The R^2 values of ISO-BPNN for T4, T5, O_2

Table 5: Test functions.

Function number	Function name	Domain of definition	Theoretical optimal value
TF1	Sphere	(−100, 100)	0
TF2	Schwefel's P2.22	(−10, 10)	0
TF3	Schwefel's P1.2	(−100, 100)	0
TF4	Rosenbrock	(−1.28, 1.28)	0
TF5	Rastrigin	(−5.12, 5.12)	0
TF6	Ackley	(−32, 32)	0
TF7	Griewank	(−600, 600)	0
TF8	Schwefel's P2.26	(−500, 500)	−12569.50

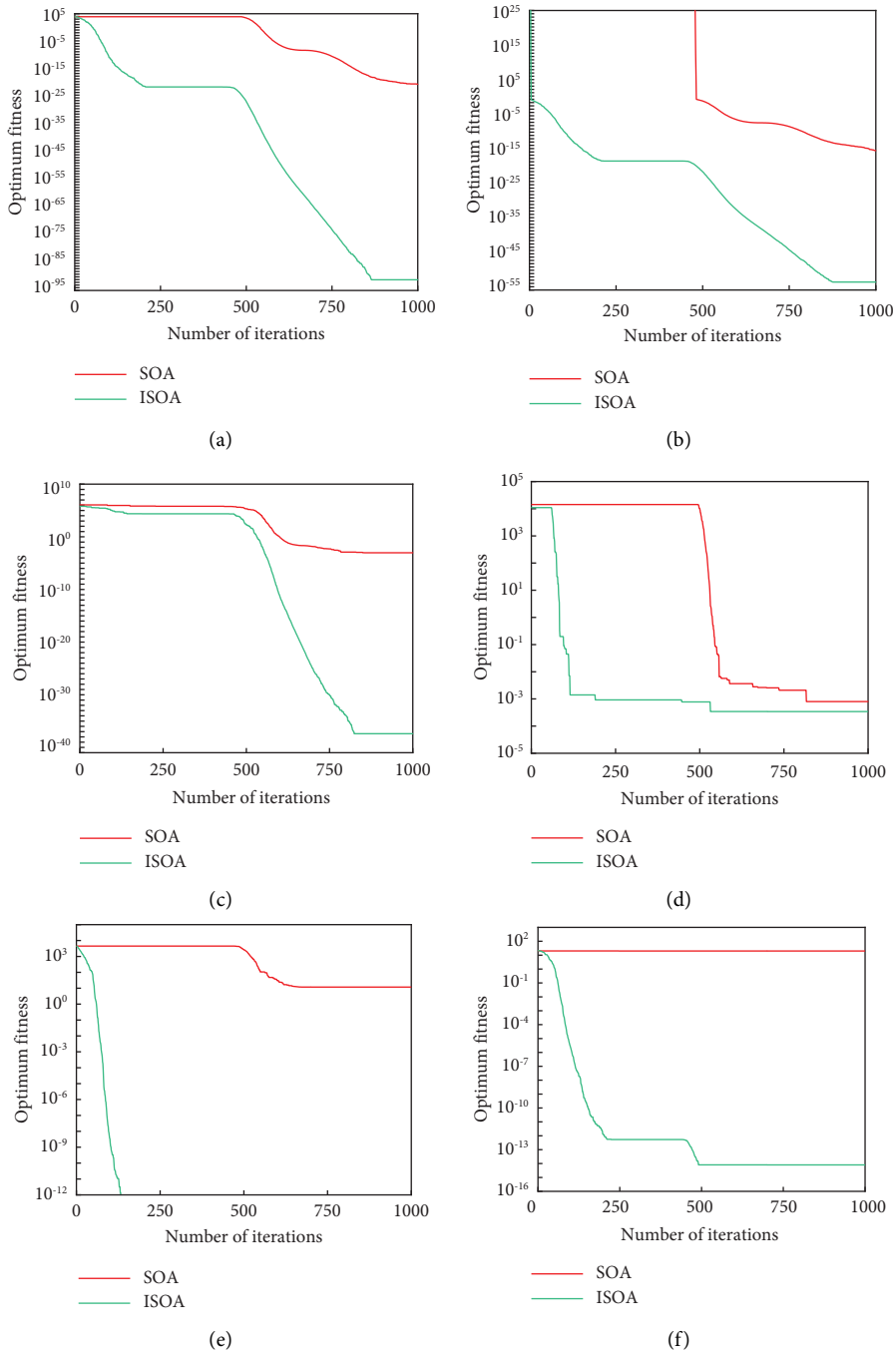

Figure 9: Continued.

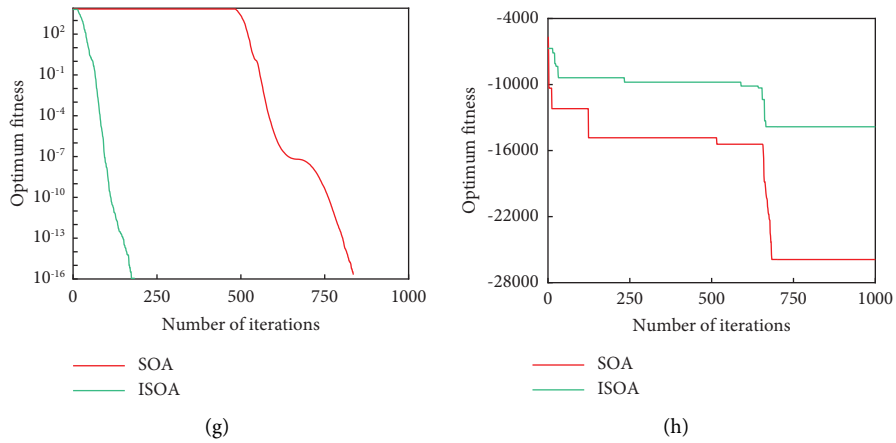

Figure 9: Comparison of optimal fitness before and after improvement. (a) TF1. (b) TF2. (c) TF3. (d) TF4. (e) TF5. (f) TF6. (g) TF7. (h) TF8.

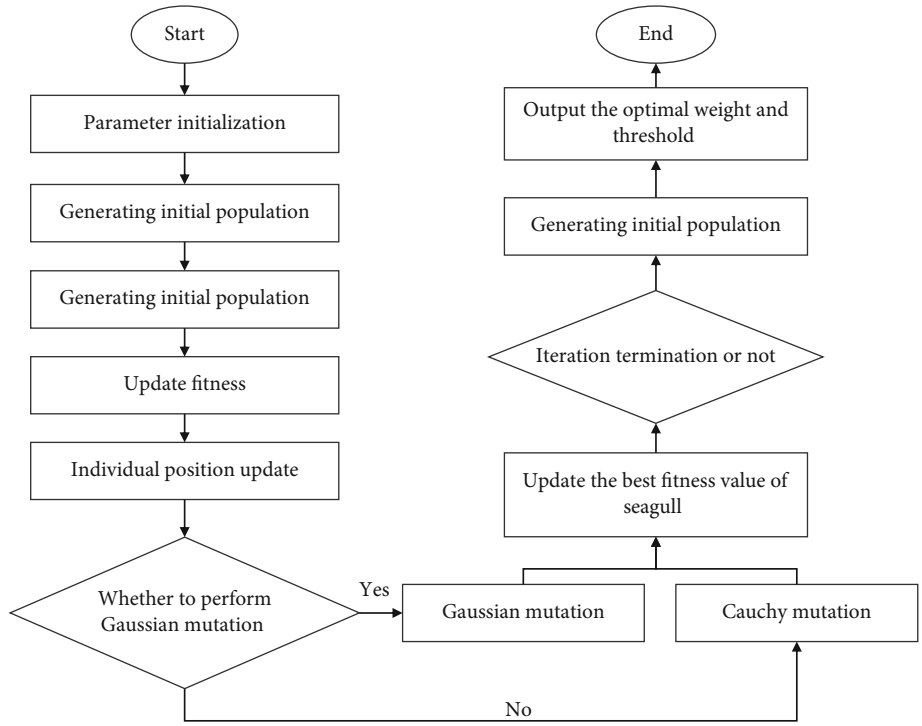

Figure 10: Model optimization procedure.

concentration, NO_x, smoke, BSFC, and turbine inlet temperature are 0.97, 0.99, 0.95, 0.99, 0.96, 0.99, and 0.98, respectively. The prediction error of ISOA-BP is smaller than that of SOA-BP. The prediction effect of ISOA-BP on O_2 concentration and smoke is significantly improved. ISOA improves the linearity of the fit of the BPNN model and reduces the fitting error. Therefore, the prediction effect of ISOA-BPNN is better than SOA-BPNN. ISOA effectively optimizes the initial connection weights and thresholds of BPNN, making it closer to the theoretical optimal weights and thresholds at the beginning of the algorithm iteration.

4. Multiobjective Optimization Method

Many control parameters affect the regeneration temperature of DPF. The calibration efforts must align with the demands of multiple objectives, encompassing considerations such as economy, emission levels, power performance, and safety. Finding a set of control parameters to make all optimization objectives reach the optimal level is difficult. Therefore, different optimization objectives need to be balanced to obtain a set of compromise control parameters. To address the inefficiency and high costs

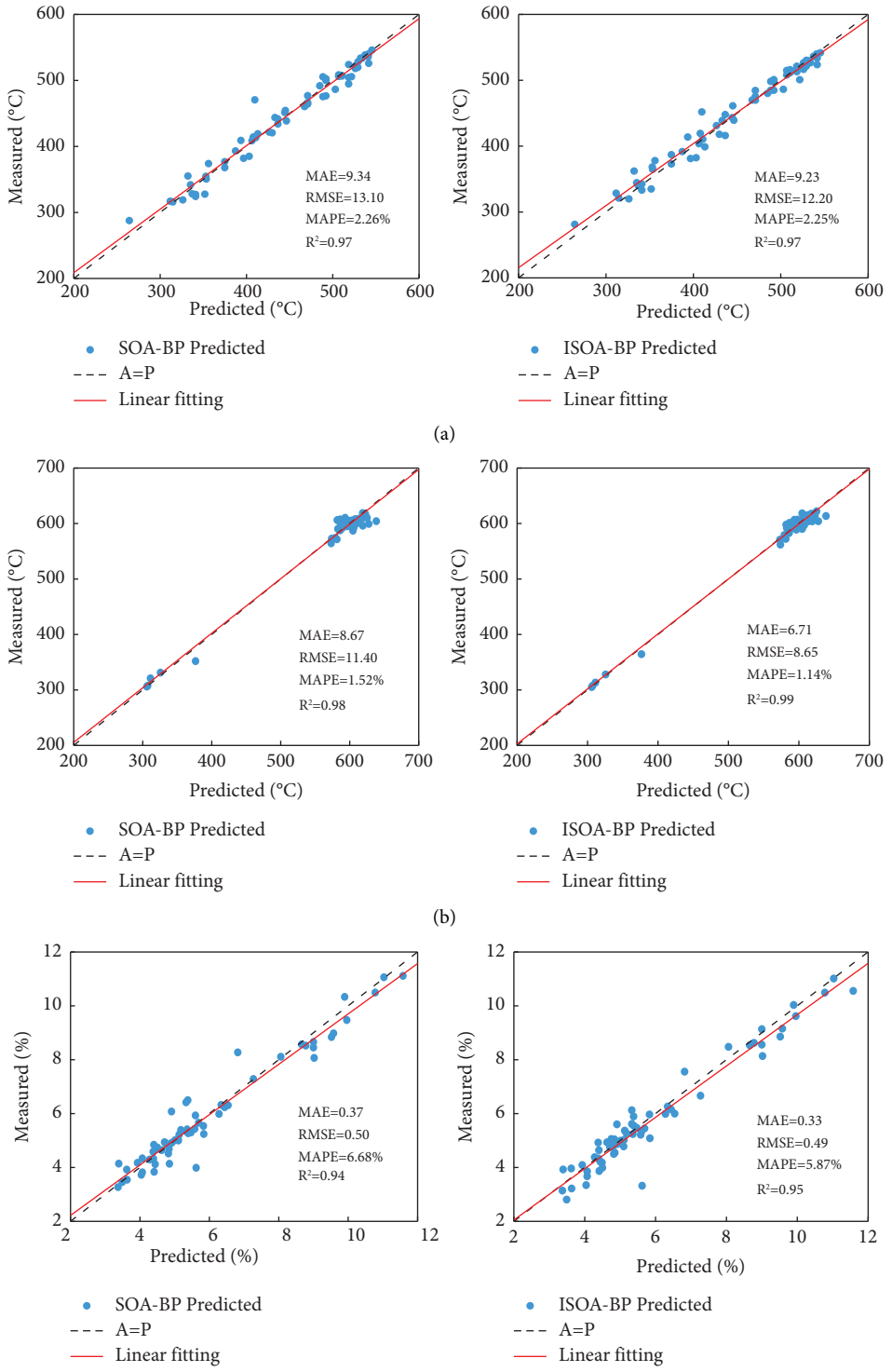

Figure 11: Continued.

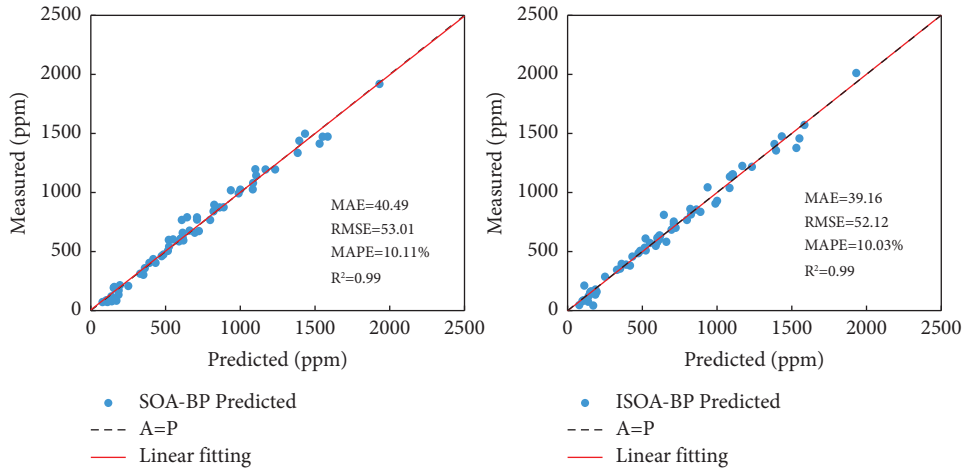

(d)

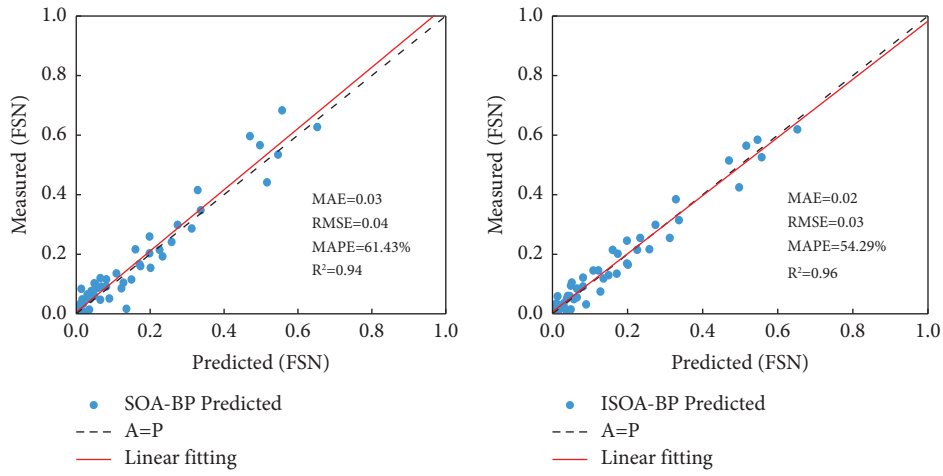

(e)

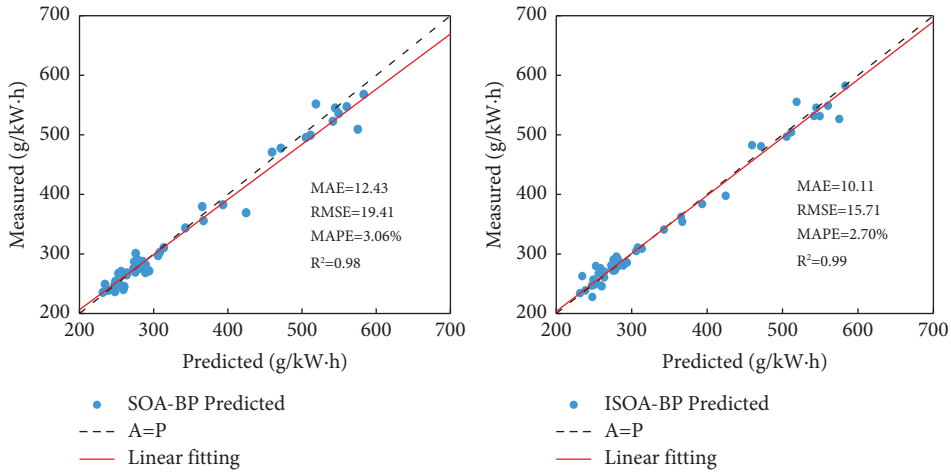

(f)

Figure 11: Continued.

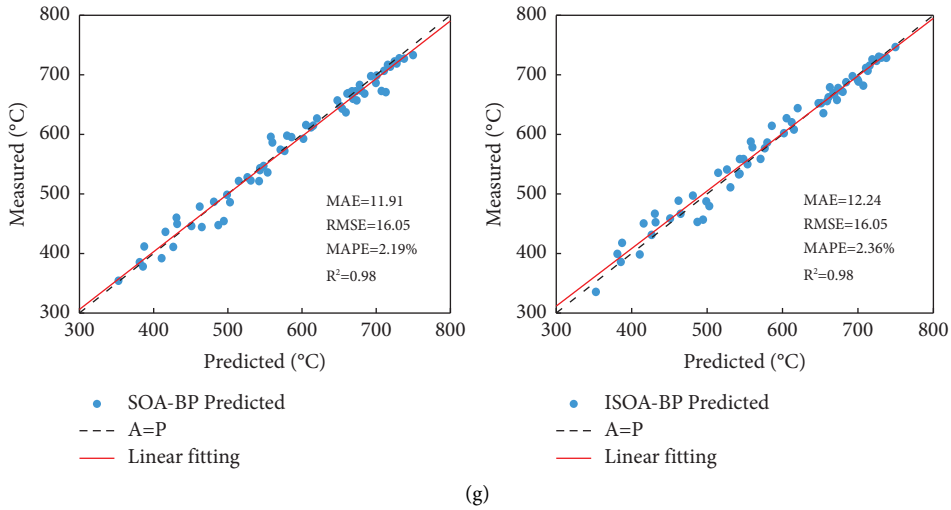

FIGURE 11: Comparison of model performance before and after improvement. (a) T4. (b) T5. (c) O_2. (d) NO_x. (e) Smoke. (f) BSFC. (g) Turbine inlet temperature.

associated with the conventional manual calibration method, an intelligent optimization algorithm is employed to optimize multiple control parameters influencing the conditions of DPF regeneration. The optimization of DPF regeneration conditions includes the calibration of regeneration temperature T4 and regeneration temperature T5. A multiobjective optimization problem between the control and performance parameters of the DPF regeneration temperature is investigated in this section based on NSGA-III.

4.1. Constraint Condition. DPF regeneration condition optimization is a process of multiobjective optimization of control parameters. The primary purpose is to ensure that the temperature entering the DPF is high enough to burn the particles in the DPF thoroughly. The optimization of DPF regeneration conditions is to calibrate the T4 temperature and T5 temperature while ensuring O_2 concentration in the exhaust. By adjusting the control parameters of the fuel system and air system, T4 and T5 can reach the target demand temperature to ensure that the DPF regeneration process can be conducted efficiently. The required temperature of T4 is 500 ± 50°C. When the exhaust temperature is low at low speed and low load, the requirements can be relaxed, but the temperature must be greater than 200°C to ensure the normal ignition of DOC. The demand temperature for T5 is 620 ± 20°C.

The condition of DPF regeneration is not only temperature but also sufficient O_2 to participate in the oxidation reaction. Therefore, ensuring enough O_2 in the exhaust gas entering the retreatment system is necessary. In the regeneration mode, the O_2 concentration of exhaust is required to be greater than 4%–5%. At low speed and high load, due to the small air-fuel ratio, the remaining oxygen in the cylinder combustion is less, so the requirement of O_2 concentration can be appropriately reduced by 2%~3%.

During the T4 calibration, the fuel can burn as thoroughly as possible in the cylinder. On the one hand, the leaked HC will oxidize in DOC, resulting in a sharp rise in the DOC temperature and even destroying the DPF. On the other hand, the increase in exhaust temperature caused by the leaking HC is uncontrollable. It will interfere with the controller's thermal management process in the aftertreatment system and will cause oil dilution. Therefore, the temperature rise of DOC is required to be less than 100°C.

During the calibration process, adjustments to fuel injection and intake control parameters can alter the air-fuel ratio and combustion temperature within the cylinder, leading to increased particulate matter emission. Therefore, the maximum limit of the smoke exhaust degree is set to 2 FSN, which can be set to 2.5 FSN at low speed and high load. A high temperature in the cylinder and oxygen-rich combustion will also lead to increased NO_x emissions. Therefore, NO_x emissions should also be considered in the calibration process. In the T5 calibration process, the turbine inlet temperature control is an essential process of regeneration condition calibration. If the exhaust temperature exceeds the limit (750°C), the excessive temperature which spikes inside the DPF may melt down the filter. During calibration, the turbine inlet temperature is controlled within 720°C.

Therefore, the purpose of the DPF regeneration calibration is to ensure that the exhaust O2 content reaches the required value while the T4 and T5 temperatures reach the required value. The rise in DOC temperature is slight, the vortex front temperature is lower than the set value, and smoke, BSFC, and NO_x are as low as possible.

4.2. Objective Function. The objective function is the fitness function of multiobjective optimization of DPF regeneration conditions. The objective function is a tool to evaluate the

quality of each individual in the iterative process of the NSGA-III algorithm. The cost function of T4 calibration is

$$\begin{aligned} C_{T4}\left(X^T\right) &= \left[c_1\left(X^T\right), c_2\left(X^T\right), c_3\left(X^T\right), c_4\left(X^T\right), c_5\left(X^T\right)\right]^T, \\ X^T &= \left[x_1, x_2, x_3, x_4, x_5, x_6, x_7, x_8, x_9, x_{10}\right]^T, \end{aligned} \tag{23}$$

where $c_1(X^T) \sim c_5(X^T)$ are the corresponding objective functions of T4, exhaust O_2 concentration, NO_x, smoke, and BSFC, respectively, and X^T is the point of speed, torque, preinjection timing, preinjection fuel quantity, main injection timing, rear injection 2 timing, rear injection 2 fuel quantity, rear injection 1 fuel quantity, rail pressure, and intake gas demand value in the 10-dimensional space.

The constraint conditions in the T4 calibration process are

$$\left.\begin{aligned} G_1\left(X^T\right) &= g_1\left(X^T\right) - g_{1\lim} \geq 0 \\ G_2\left(X^T\right) &= g_2\left(X^T\right) - g_{2\lim} \geq 0 \\ G_3\left(X^T\right) &= g_3\left(X^T\right) - g_{3\lim} \leq 0 \\ G_4\left(X^T\right) &= g_4\left(X^T\right) - g_{4\lim} \leq 0 \\ g_6\left(X^T\right) &= g_1\left(X^T\right) \leq 50 \end{aligned}\right\}, \tag{24}$$

where $g_1(X^T) \sim g_4(X^T)$ are the model predicted outputs corresponding to T4, exhaust O_2 concentration, NO_x, and smoke; $g_6(X^T)$ is the model prediction output corresponding to T5; and $g_{1\lim} \sim g_{4\lim}$ are the limits of T4, exhaust O_2 concentration, NO_x, and smoke.

The cost function of T5 multiobjective optimization is

$$C_{T5}\left(X^T\right) = \left[c_5\left(X^T\right), c_6\left(X^T\right)\right]^T, \tag{25}$$

where $c_6(X^T)$ is the target function corresponding to T5.

The constraint conditions in the calibration process of T5 are

$$\left.\begin{aligned} G_5\left(X^T\right) &= g_5\left(X^T\right) - g_{5\lim} \leq 0 \\ G_6\left(X^T\right) &= g_6\left(X^T\right) - g_{6\lim} \geq 0 \end{aligned}\right\}, \tag{26}$$

where $g_5(X^T)$ is the model output of BSFC and $g_{5\lim}$ and $g_{6\lim}$ are the limits corresponding to BSFC and T5.

The optimization of the DPF regeneration condition solves the control parameter combination corresponding to the minimum of each object. Therefore, the multiobjective optimization problem of DPF regeneration conditions can be transformed into the problem of solving the minimum value of the cost function $C(X)$. The mathematical description of the optimization problem is

$$F\left(X^T\right) = \begin{cases} \min\left(C_{T4}\left(X^T\right)\right) \\ \min\left(C_{T5}\left(X^T\right)\right). \end{cases} \tag{27}$$

After optimization by the NSGA-III algorithm, the Pareto optimal solution set corresponding to the minimum cost function $C_{\min}(X)$ is generated. Each point in the solution set represents a set of optimal control parameter combinations X^T. The final calibration results can be selected from the optimal control parameter combination set according to the requirements of different operating conditions.

4.3. The Multiobjective Optimization Method Based on the NSGA-III Coupled with ISOA-BP. The optimal calibration of DPF regeneration conditions is based on ISOA-BP and NSGA-III. The ISOA-BP prediction model verifies the optimal set of NSGA-III. Suppose the error of the optimization results does not meet the requirements; the new data of the engine model will be integrated with the training data of the previous cycle of the optimization process. Then, the ISOA-BP model is trained again with the new integrated training data. This optimization training method can be defined as the cyclic optimization method. The ISOA-BP model is trained repeatedly with the increase of training data. Once the error is satisfied, the final Pareto optimal set will be obtained by the final ISOA-BP model. The cyclic optimization method streamlines the workload, simultaneously enhancing model prediction accuracy and precisely identifying the optimal operating parameters. In the ISOA-BP model, the input corresponds to the parameter targeted for optimization, and the output represents the performance evaluation parameter. The optimization of DPF regeneration conditions includes the calibration of regeneration temperature T4 and regeneration temperature T5. During calibration, the original control parameter is used as the reference point. This default reference point is considered as the optimal control parameter, and the search is conducted for the best control parameter close to the reference point. The scope is then expanded and the search continues if the optimal control parameter is not found. After iterative calculation, the Pareto optimal solution set satisfying all optimization objectives is finally obtained.

DPF regeneration conditions are optimized for the speed range of 1000 r/min–2800 r/min and the load range of 10%–90%. According to the speed interval (every 200 r/min, an operating point) and the load interval (every 10%, an operating point), 100 calibration working points are set. After setting the initial search range of all parameters, the automatic calibration of scanning points can be started one by

one. After the calibration is completed, the calibration results will be checked. The search range will be reset before calibration if the results do not meet the calibration requirements. The steps of the multiobjective optimization program are shown in Figure 12.

The final output of the NSGA-III algorithm is a solution set. Therefore, it is necessary to select a set of optimal control parameters. For example, at 1600 r/min speed and 100% load, the three sets of data from the calibration results are shown in Table 6. The smoke and NO_x emissions in group 1 are more significant than those in the other two groups, and the O_2 concentration is lower, but the T4 temperature is the highest. Elevating the T4 temperature is associated with increased smoke and NOx emissions while concurrently reducing the O2 concentration. Achieving the optimal target for all these parameters is challenging due to these interconnected effects. There is a contradiction between each calibration target under different working conditions. Therefore, it is necessary to determine the optimal solution from the solution set based on the actual situation and the demand of each target.

In order to find the optimal solution in the solution set, each target is assigned a weight ω. The weighted summation of each target parameter is calculated. The final result is the control parameter corresponding to the smallest value after the weighted summation in the nonsolution set. The weighted summation formula is

$$S = \sum_{i=1}^{n} \omega_i \frac{g_i(X^T) - g_{\min i}(X^T)}{g_{\max i}(X^T) - g_{\min i}(X^T)}, \tag{28}$$

where ω_i is the weight of each target in the calibration process of T4 and T5. $|\omega_i| \leq 1$, that is, the sum of the absolute values of the weights is equal to 1. $g_{\max i}(X^T)$ and $g_{\min i}(X^T)$ are the maximum and minimum values of the target parameters in the noninferior solution set, respectively.

We then input the optimized parameters into the predictive model for simulation validation. Due to the abundance of optimized operating points, only one steady-state operating condition is presented here for simulation validation. A comprehensive experimental validation of the simulation results across all operating conditions will be conducted in the next chapter. The parameters and response changes of the engine before and after optimization under the operating conditions of 1800 r/min and 120 Nm are shown in Table 7

After optimization, the most significant change in fuel injection parameters is observed in the quantity of rear injection 2, which decreased by 21.1%. Rear injection 1's quantity increased by 20.5%c. Both the main injection timing and preinjection quantity have slightly advanced. T4 and T5 temperatures have increased, with T5 experiencing a slightly lower increase. O_2 concentration has risen by 1.8%. NO_x and smoke emissions have decreased by 80.82 ppm and 0.31 FSN, respectively. BSFC has decreased by 27 g/kW·h. After optimization, emissions and fuel consumption have been reduced while satisfying DPF regeneration requirements, achieving emission reduction goals, and improving fuel efficiency.

5. Results and Discussion

5.1. Steady-State Experiments Based on the Mapping Characteristics for Validation. The NSGA-III algorithm is employed to optimize the global calibration of the fuel injection MAP at varying engine speeds from 1000 to 2800 r/min and under loads ranging from 0% to 100%. Subsequently, the optimized MAP values are written into the original ECU using calibration software to validate the effectiveness of the multiobjective optimization results. A comparison before and after T4 temperature optimization is shown in Figure 13. The variation trend of T4 before and after optimization is the same. In the DPF regeneration mode, T4 improved significantly at low speed and low load. T4 minimum temperature increased from 222°C to 270°C. At low speed and low load, the increase in T4 temperature means that DOC has better ignition conditions. In the diesel engine speed range of 1200 r/min~1600 r/min, after optimization, the T4 temperature at high load reached the optimal temperature (500 ± 50°C), and the optimal T4 temperature area covered more operating points than before optimization. The T4 temperature reaches above 500°C at more operating points at high speed and load in diesel engines. T4 temperature is improved at medium and high speeds so that the additional HC provided by the rear injection can be oxidized more efficiently during the regeneration of DPF. The average value of T4 in all operating conditions increased from 446°C to 460°C, with an overall increase of 3.14%.

A comparison of exhaust oxygen concentrations before and after optimization is shown in Figure 14. The O_2 concentration at low speed and high load before the optimization is lower than the required value at some operating points, which is not conducive to the oxidation reaction of the after-treatment system. After optimization, the oxygen concentration in the low-speed and high-load areas is improved, and the minimum oxygen concentration is increased from 1.05% to 2.91%. At low-speed and high-load conditions, the O_2 concentration of the exhaust exceeds the requirement limit by more than 2%–3%, and the O_2 concentration in other conditions is greater than 4%–5%. All the optimized operating points meet the calibration requirements. The average O_2 concentration in all operating conditions increased from 5.19% to 5.75%, with an overall increase of 10.79%.

The comparison before and after NO_x optimization is shown in Figure 15. The optimization effect of NO_x is more evident at the high-load condition in the speed range of 1200 r/min~2400 r/min. The operating point with NO_x emission higher than 1300 ppm is significantly reduced. After optimization, the NO_x emission contour showed an upward trend compared with that before optimization, and the overall NO_x emission was reduced. The average NO_x emission in all operating conditions decreased from 788.86 ppm to 720.39 ppm, with an overall decrease of 8.68%.

The comparison before and after smoke optimization in the regeneration mode is shown in Figure 16. After optimization, the smoke intensity significantly improves in low-

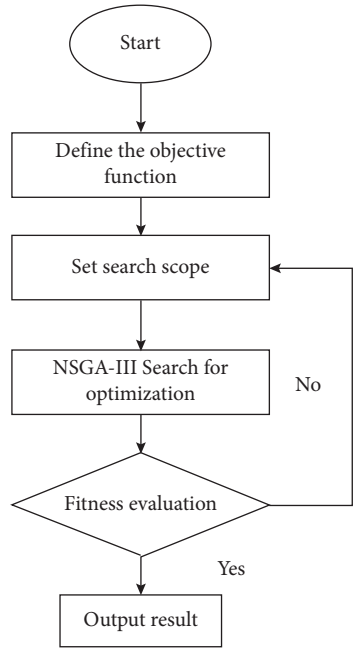

Figure 12: Multiobjective optimization steps.

Table 6: Partial calibration results at 1600 r/min and 100% load.

	Smoke (FSN)	O_2 (%)	NO_x (ppm)	T4 (°C)
1	0.71	2.84	1398	491
2	0.63	4.38	1287	477
3	0.17	5.84	1084	448

Table 7: Comparison of parameters and responses before and after optimization.

Parameter	Before optimization	After optimization	Percentage change
Preinjection quantity (mg)	1.90	1.80	−5.23%
Rear injection 1 quantity (mg)	3.84	4.36	20.5%
Rear injection 2 quantity (mg)	8.88	7.00	−21.1%
Rear injection 2 timing (°CA)	−42.47	−43.88	−1.41
Main injection timing (°CA)	9.25	8.92	−3.5%
Preinjection timing (°CA)	18.06	13.60	−20.7%
T4 (°C)	433.06	474.32	9.5%
T5 (°C)	592.56	600.19	1.3%
O_2 (%)	4.44	5.24	18.5%
NO_x (ppm)	428.57	347.75	−18.8%
Smoke (FSN)	1.17	0.86	−26.5%
BSFC (g/kW·h)	326.00	353.00	8.3%

speed and high-load areas and the range of the red regions with smoke emissions greater than 2 FSN is significantly reduced. The maximum smoke emission decreased from 2.78 FSN to 2.42 FSN. The smoke emission of medium and low loads is significant. After calibration and optimization, the smoke emission of this part of operating conditions is reduced, especially when the speed is 1600 r/min-~2400 r/min and the load is 25%–50%. The average smoke density in all operating conditions decreased from 0.58 FSN to 0.51 FSN, with a decrease of 12.07%. Figure 17 shows the DOC temperature rise verification after T4 calibration. The optimized parameters meet the requirements of DPF regeneration conditions. The overall temperature increase of the DOC remains below the maximum limit, ranging between 0°C and 40°C.

A comparison of the regeneration temperature T5 before and after optimization is shown in Figure 18. The T5 temperature of medium-load and high-load conditions at low rotational speed increased to more than 550°C, significantly improving compared to before calibration. The

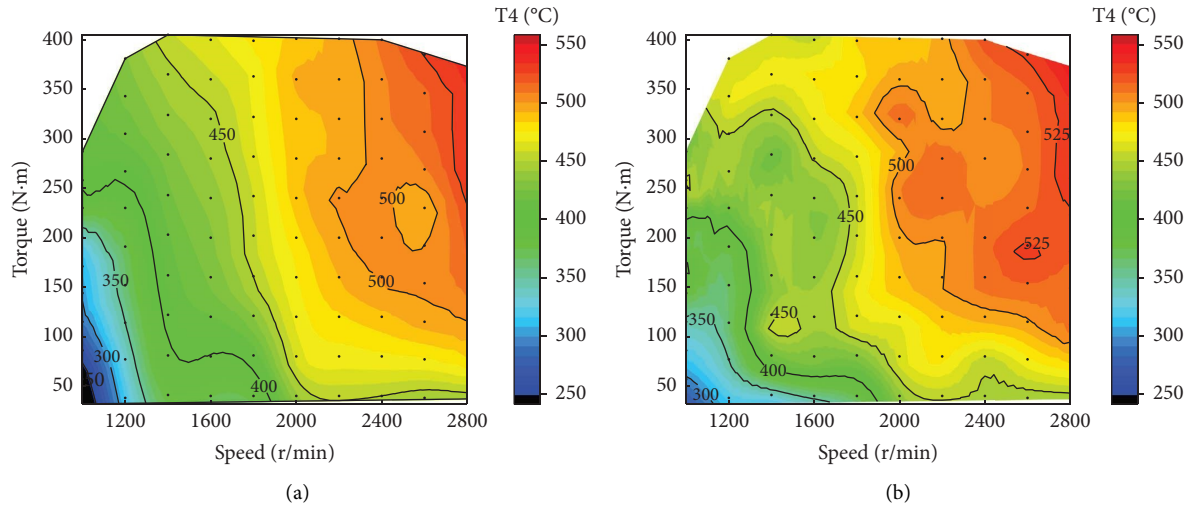

Figure 13: Comparison of T4 temperature (a) before and (b) after optimization.

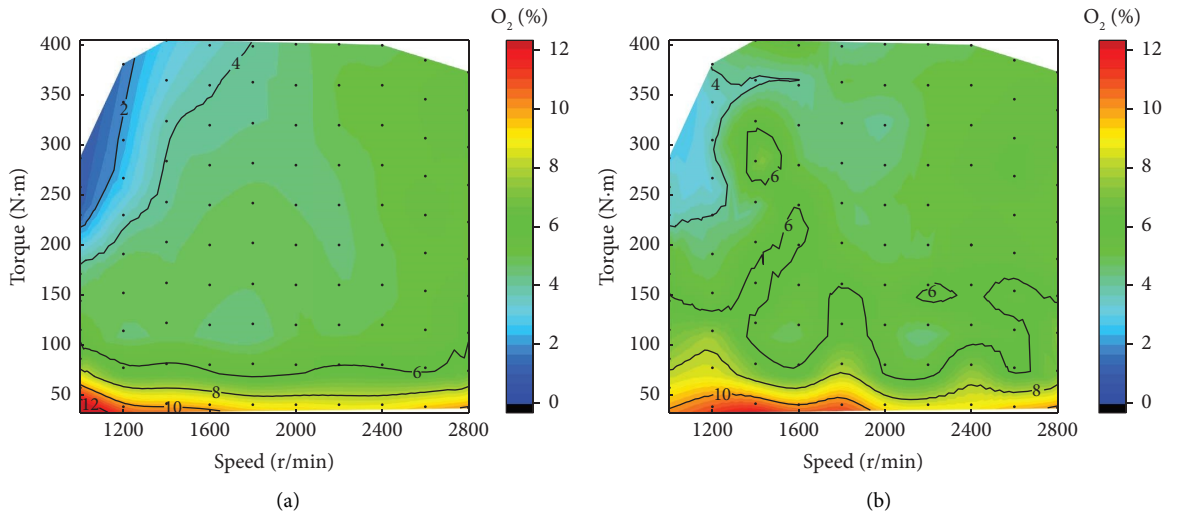

Figure 14: Comparison of O_2 temperature (a) before and (b) after optimization.

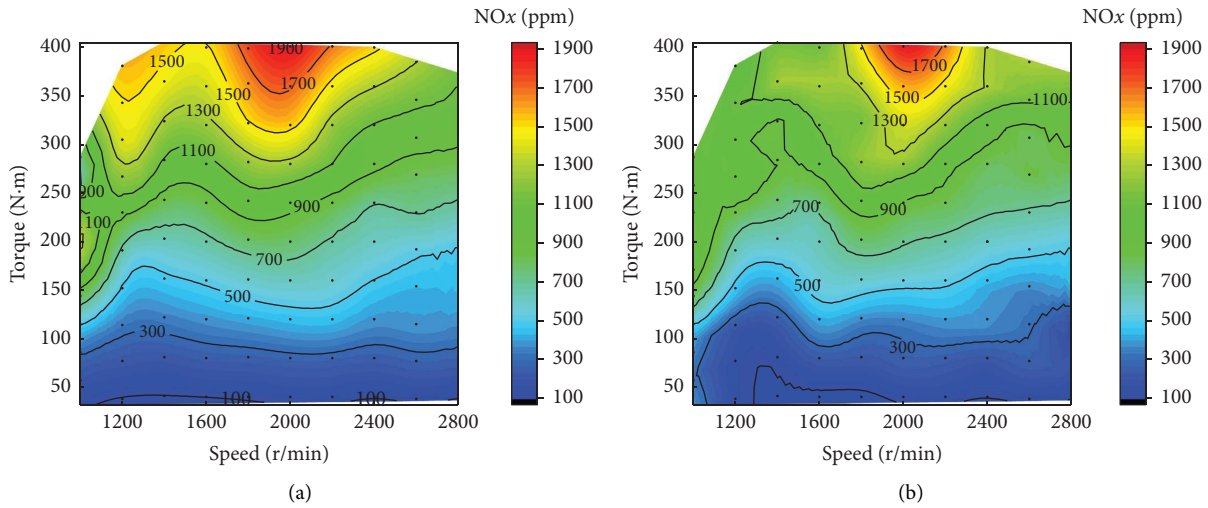

Figure 15: Comparison of NO_x temperature (a) before and (b) after optimization.

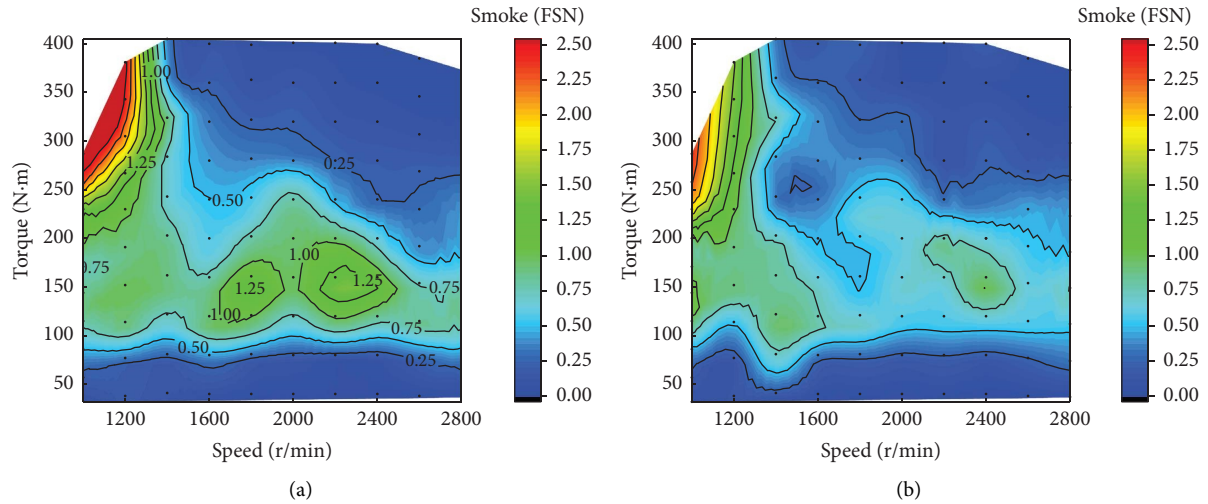

Figure 16: Comparison of smoke temperature (a) before and (b) after optimization.

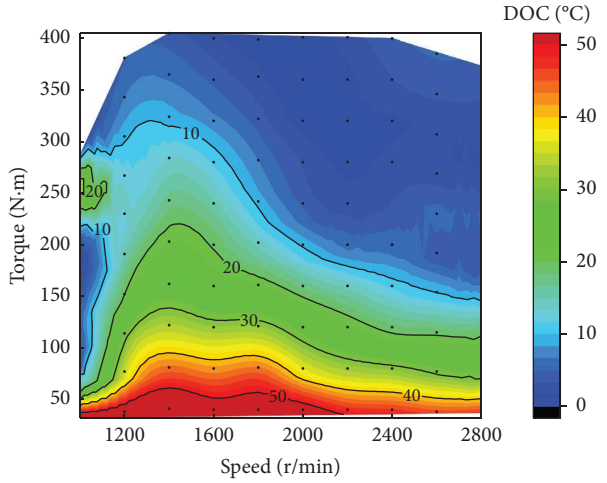

Figure 17: DOC temperature verification.

optimal operating interval of T5 is 620°C ± 20°C, and more operating points are in the optimal operating area of T5 after optimization. During the DPF regeneration, the soot can be cleaned efficiently in more operating conditions. The average regeneration temperature T5 in all operating conditions increased from 580°C to 592°C, with an increase of 2.07%.

The comparison of BSFC before and after optimization is shown in Figure 19. The contour line with BSFC of 250 g/kW·h moves down obviously. Therefore, the BSFC is reduced to a certain extent under high load, and the BSFC is improved when T5 is not reduced. The average value of all operating conditions of BSFC decreased from 317.89 g/kW·h before optimization to 314.63 g/kW·h after optimization, with a decrease of 1.03%.

The optimized turbine inlet temperature is shown in Figure 20. The maximum value of turbine inlet temperature is 720°C, and DPF can normally regenerate when the turbine inlet temperature is lower than the value. After calibration and optimization, the turbine inlet temperature does not exceed the limit in all operating conditions, and the maximum temperature is 714°C. Therefore, the DPF can be safely regenerated under all operating conditions.

5.2. Experimental Verification of DPF Regeneration. In order to verify the influence of the optimized parameters on the actual DPF regeneration process, DPF active regeneration experiments were carried out on the engine test bench. The loading condition is 1000 r/min and 100% load. Active regeneration experiments were conducted on the engine test bench to assess the impact of the optimized parameters on the actual DPF regeneration process. For comparison results, the regeneration was performed under the operating conditions of 1400 r/min and 350 Nm, which represent the area with the most noticeable improvement in T4. Two groups of injection parameters before and after optimization

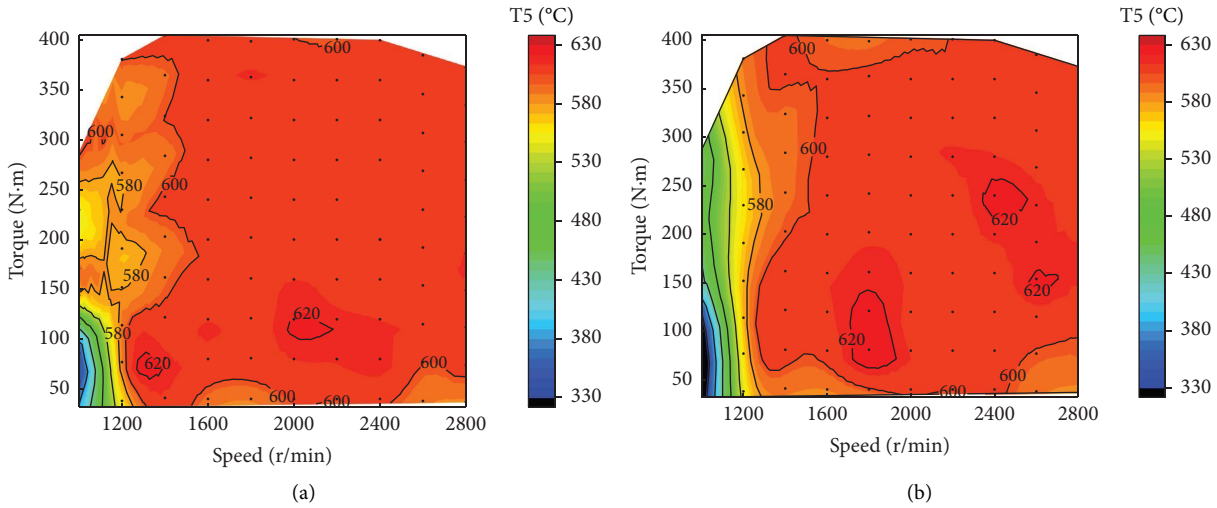

Figure 18: Comparison of T5 temperature (a) before and (b) after optimization.

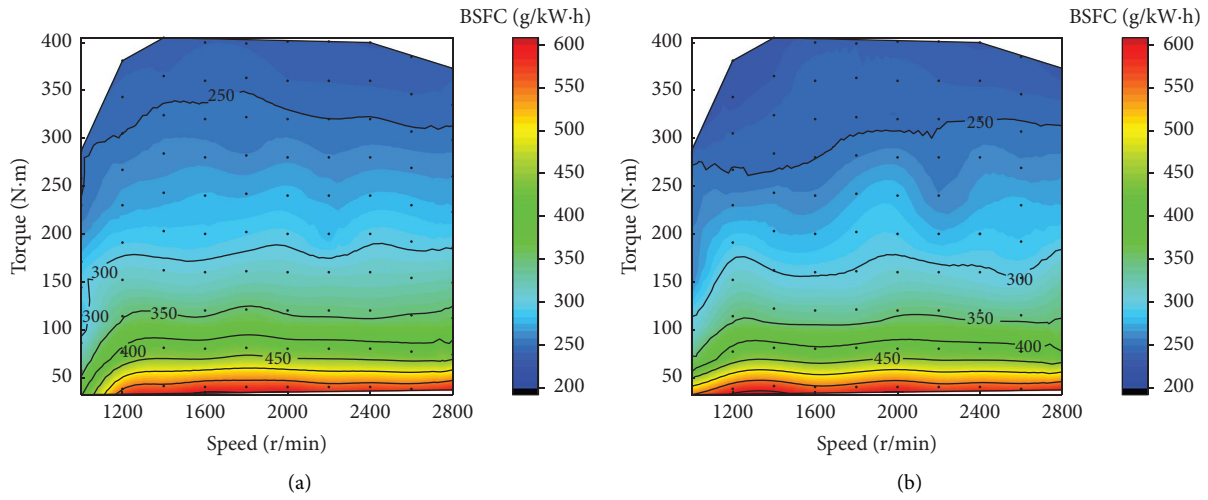

Figure 19: Comparison of BSFC (a) before and (b) after optimization.

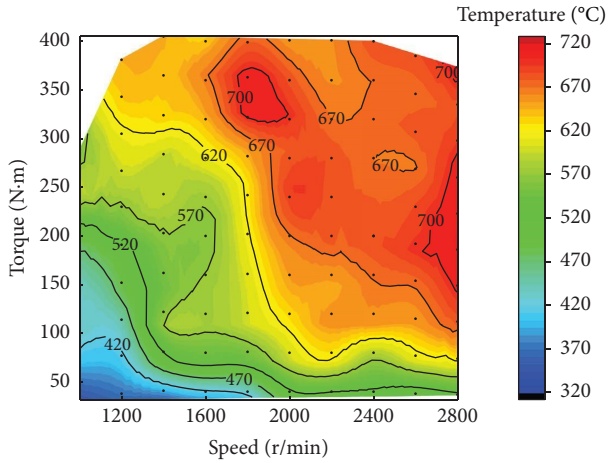

Figure 20: Comparison of turbine inlet temperature before and after optimization.

were written into the ECU, and two active regeneration experiments were carried out. The regeneration time was 1200 s. The regeneration effect is evaluated for the parameters before and after optimization, and the regeneration efficiency is defined as η as follows:

$$\eta = \frac{M_a - M_b}{M_a - M} \times 100\%, \tag{29}$$

where M_a and M_b are the carrier mass before and after regeneration, respectively, and M is the carrier net mass.

Figure 21 shows the active regeneration efficiency and maximum carrier temperature before and after optimization. After optimization, the DPF regeneration efficiency reaches 88.2%, which is 18.9% higher than before. Since the optimization not only increases the temperature of T4 and T5 but also increases the O2 concentration, it regenerates in the best operating area. According to 21 (b), compared with before optimization, not only is the peak temperature of the carrier increased but also the temperature rise rate is increased. The maximum temperature of the carrier is 711.8°C before optimization and 780°C after optimization. Therefore, the injection parameters after multiobjective optimization can improve the DPF regeneration efficiency and increase the carrier's combustion temperature under the condition of carrier safety. Therefore, it is proved that the multiobjective optimization method is effective in the actual DPF regeneration process.

5.3. WHTC Cycle Test Verification. To verify the transient DPF regeneration conditions and engine performance after optimization, the worldwide harmonized transient cycle (WHTC) was used to verify the engine regeneration performance after optimization. Each cycle consists of 1800 transient test cycles, with conditions changing every second. The speed and torque changes of WHTC during operation are shown in Figure 22. The engine was configured in regenerative mode, and WHTC tests were carried out based on the fuel injection control parameters before and after optimization. Thus, the engine regeneration performance under transient conditions was analyzed and verified.

The comparison of T4 and T5 before and after optimization is shown in Figure 23. After optimization, there is a noticeable enhancement in both T4 and T5 temperatures, particularly under idle low-load conditions where T4 temperatures were previously lower. Before optimization, T4 temperature is mainly distributed between 180°C and 350°C. After optimization, there is a significant overall temperature increase, with most operating points now distributed between 250°C and 420°C. The average temperature of the whole cycle increased from 261°C to 342°C. The average temperature of T4 in the transient state is lower than that in the steady state. Since most of the WHTC is in the low-temperature area of low load, the average T4 temperature is low. T5 is promoted more obviously in the low-speed and high-load operation areas, most of which are between 550 and 600°C. This ensures that carbon inside the carrier is efficiently cleaned during DPF regeneration. The T5 optimization effect is not apparent at the high engine speed and torque operating point. The optimization successfully raises the average temperature of the entire cycle from 577°C to 592°C, ensuring improved emissions control and fuel efficiency, especially meeting the requirements for T5. The comparison of O_2 concentration before and after optimization is shown in Figure 24. Before optimization, O_2 concentration in some operating conditions is low, which is not conducive to DOC oxidation reaction. After optimization, the O_2 concentration in low O_2 concentration conditions is significantly increased, and thus all conditions meet the demand for regeneration.

Since the condition changes rapidly in the WHTC cycle, the recorded results change second by second. Therefore, the AVL414 smoke meter used in a steady state is inaccurate in measuring the transient smoke change. The AVL415 smoke meter intercepts particulate matter using filter paper and then utilizes laser illumination on the filter paper to calculate smoke opacity based on its light transmittance. Therefore, the AVL483 smoke meter is used in the WHTC cycle test. It can directly measure soot content in exhaust gas by acoustic wave theory and accurately record the soot content during transient changes. A comparison of soot before and after optimization is shown in Figure 25. The optimization effect is noticeable when the soot emission is higher. The average soot decreased from 0.062 g/h to 0.054 g/h. A comparison of NO_x before and after optimization is shown in Figure 26. The optimization effect is evident in high NO_x emission conditions, especially in high-load operation conditions at medium and high speed. There is a noticeable reduction in NO_x emissions when it exceeds 1300 ppm. The average NO_x emissions throughout the cycle decreased from 356 ppm to 319 ppm.

Real-time monitoring of fuel consumption can be seen in Figure 27. After optimization, the fuel consumption in the high fuel consumption condition is reduced, while the fuel consumption in the low fuel consumption condition is slightly increased. This is consistent with the multiobjective optimization strategy. While ensuring a sufficiently high temperature for efficient DPF regeneration, fuel consumption is minimized. The DPF pressure drop comparison before and after optimization is shown in Figure 28. The pressure drop trend aligns with that of T5, with regeneration being carried out during periods of relatively high T5 temperatures. After complete regeneration, the DPF pressure drop remains in a lower state for specific durations, which are 200 seconds, 400 seconds, 800 seconds, and 1200 seconds, respectively. With the increase of T5 temperature after optimization, the regeneration efficiency of DPF is improved, and the residual carbon smoke in the carrier is less. Therefore, the DPF pressure drop after optimization is lower than before. The average WHTC cycle values of regeneration conditions, emissions, and fuel consumption before and after optimization are shown in Table 8. Overall, the optimization of DPF regeneration conditions is evident. The proposed multiobjective optimization method proves effective in real-world transient applications, as demonstrated by the WHTC cyclic transient test.

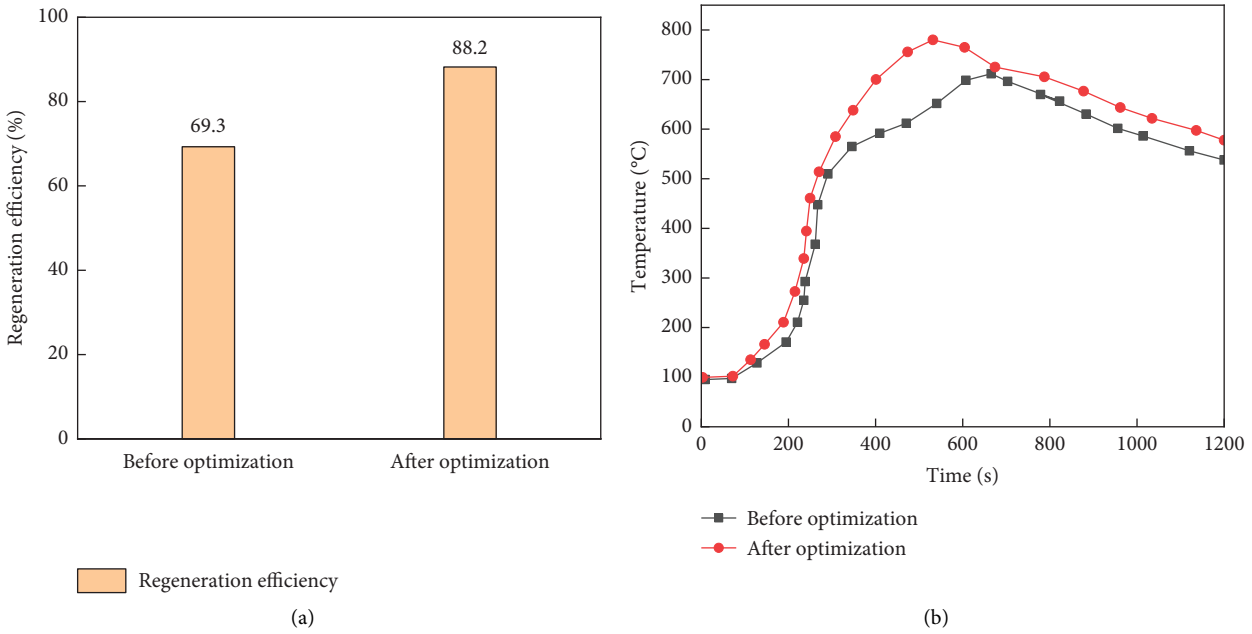

Figure 21: (a) Active regeneration efficiency and (b) maximum carrier temperature before and after optimization.

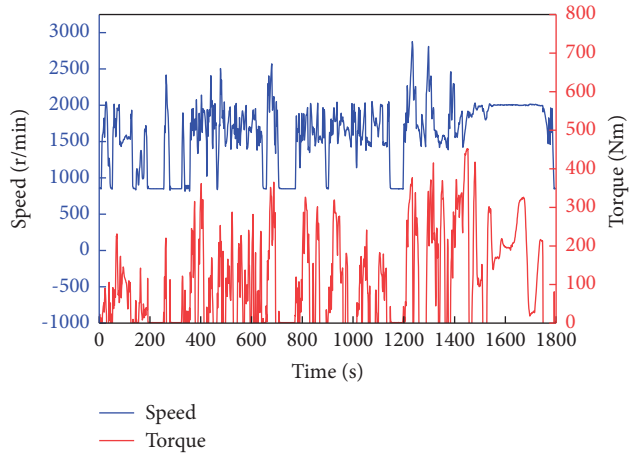

Figure 22: Standard values of speed and torque in the WHTC test cycle.

Thus, under steady-state conditions, this method has resulted in an average increase of 3.14% in DPF regeneration temperatures (T4 and T5) and exhaust oxygen concentration by 2.07% and 10.79%, respectively. Concurrently, there has been an average reduction of 8.68%, 12.07%, and 1.03% in NO_x, smoke, and BSFC, ensuring the efficient and secure regeneration of the DPF. Results from regeneration experiments indicate a DPF regeneration efficiency of 88.2%, accompanied by a temperature increase from 711.8°C to 780°C. During WHTC transient testing, there are significant improvements in T4, T5, and oxygen concentrations, with respective increases of 26%, 3.1%, and 0.5%. In addition, there are notable reductions of 10.4% and 0.8% in NO_x and smoke emissions and a 3.5% decrease in fuel consumption. These results highlight the success of the proposed cyclic optimization method, showcasing improved regeneration under steady-state conditions and significant performance gains under transient conditions. It is proved that the ISOA-BP prediction model and the NSGA-III multiobjective optimization method have apparent advantages and feasibility compared with manual calibration and provide a practical and feasible method for DPF regeneration temperature calibration and other diesel engine performance multiobjective optimization problems.

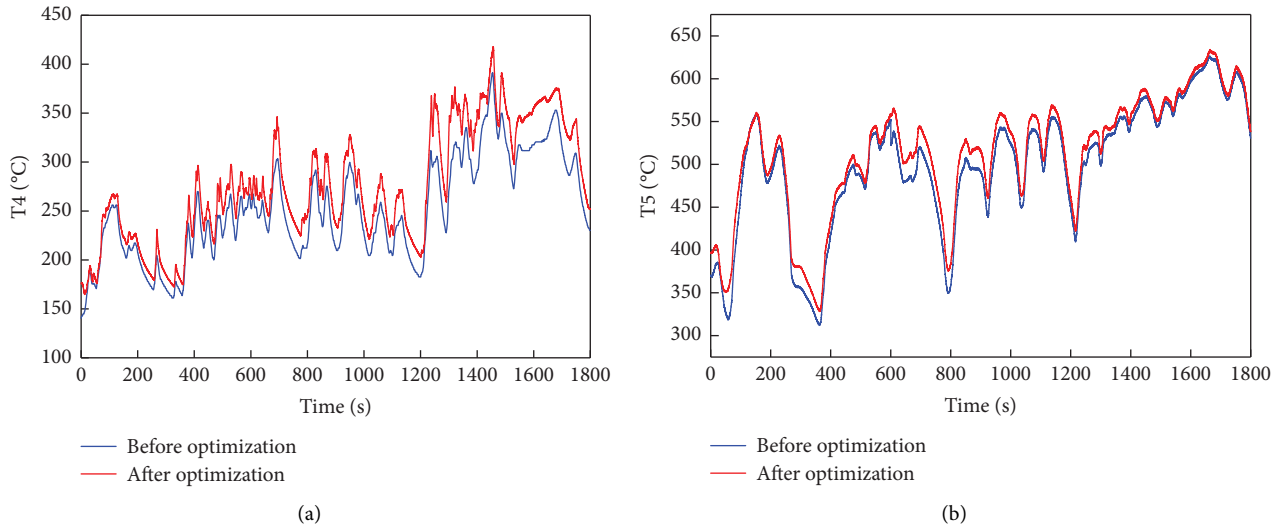

Figure 23: Comparison of (a) T4 and (b) T5 before and after optimization.

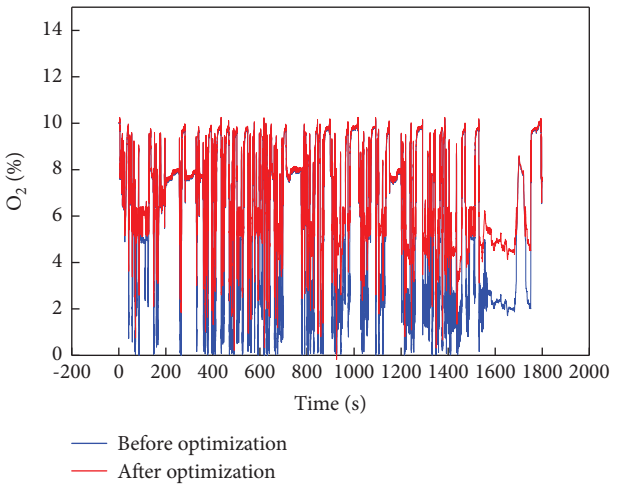

Figure 24: Comparison of O_2 concentration before and after optimization.

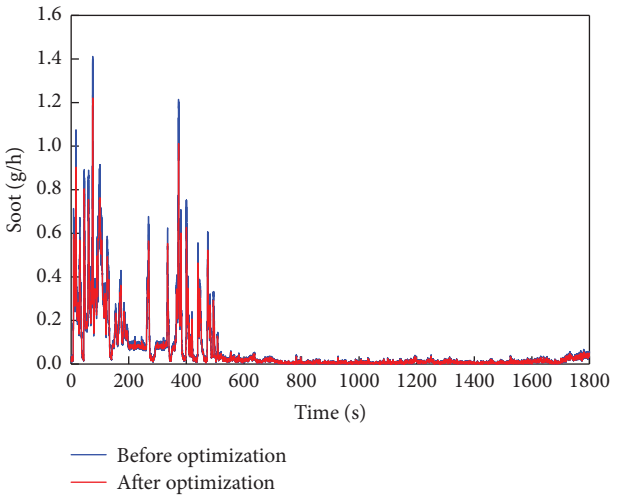

Figure 25: Comparison of soot before and after optimization.

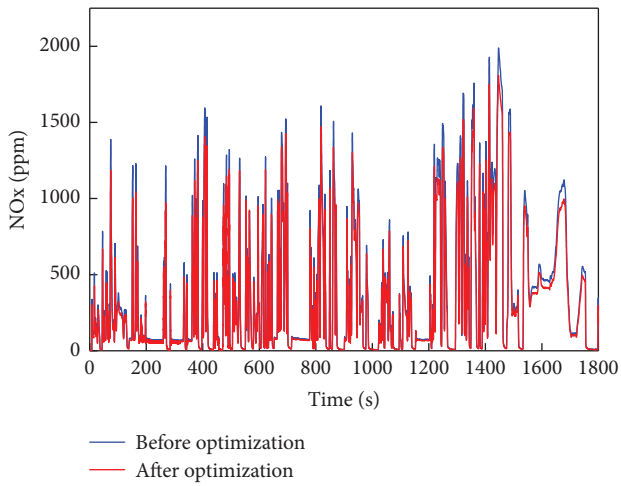

Figure 26: Comparison of NO_x before and after optimization.

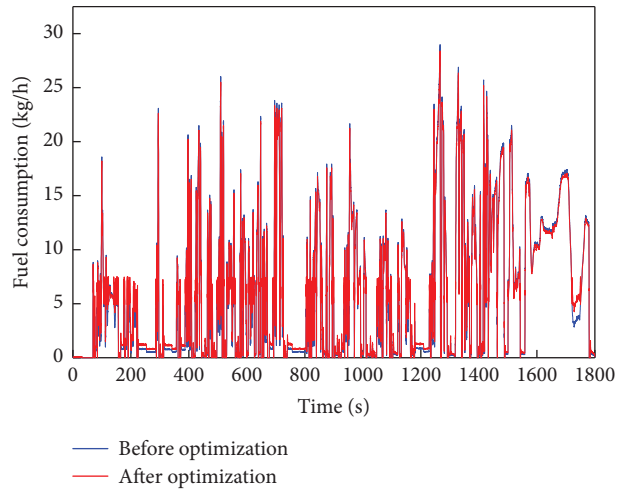

Figure 27: Comparison of fuel consumption before and after optimization.

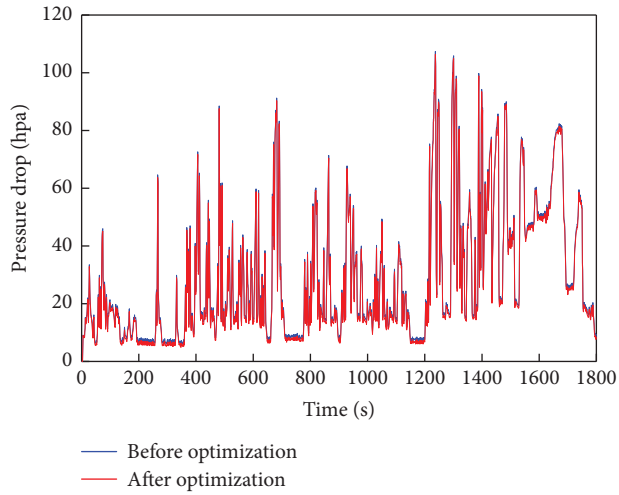

Figure 28: Comparison of DPF pressure drop before and after optimization.

Table 8: Comparison of WHTC cycle average before and after optimization.

Parameter	Before optimization	After optimization	Percentage change (%)
T4 (°C)	261	342	31.0
T5 (°C)	577	592	2.6
O_2 (%)	5.78	5.81	0.5
NO_x (ppm)	356	319	−10.4
Soot (g/h)	0.062	0.054	−0.8
Fuel consumption (kg/h)	5.65	5.56	−1.6

6. Conclusion

The optimization method presented in this study offers a promising solution for improving DPF regeneration efficiency, reducing emissions, and enhancing fuel efficiency in real-world applications. It provides an effective and viable approach for DPF regeneration temperature calibration and other multiobjective optimization challenges in diesel engine performance. The significant findings of this work are as follows:

(1) Even after SOA optimization, the BPNN model still has a significant error in predicting O_2 and smoke degrees. Before the improvement, the prediction of O_2 concentration and smoke R^2 was 0.94, and the smoke MAPE was 61.43%. The correlation of sample data is not strong, and there are noise points that interfere with the model's training and learning. In addition, the O_2 concentration and smoke level are small in the order of magnitude. Therefore, the model prediction accuracy is reduced.

(2) Based on the SOA optimization algorithm, improvements were made in four aspects: population initialization, convergence factor, iterative weight, and population mutation, resulting in the proposal of the ISOA optimization algorithm. The results demonstrate that ISOA enhances both global and local search capabilities, accelerates the convergence rate of the algorithm, and incorporates operations to escape local optima within the algorithm.

(3) The ISOA-BPNN model can solve the problem of low accuracy in O_2 and smoke prediction. Meanwhile, the prediction accuracy of other parameters is improved. The ISOA-BPNN model demonstrated superior accuracy compared to the existing SOA-BPNN model. It exhibited reduced errors and higher R^2 values across critical parameters. The R^2 values of ISO-BPNN for T4, T5, O_2 concentration, NO_x, smoke, BSFC, and turbine inlet temperature are 0.97, 0.99, 0.95, 0.99, 0.96, 0.99, and 0.98, respectively. The improved model MAPE is reduced by 0.01%, 0.38%, 0.81%, 0.08%, 7.14%, 0.36%, and 0.17%. On the existing research foundation, the accuracy of diesel engine performance prediction has been improved.

(4) The cyclic optimization method was proposed, facilitating multiobjective calibration for T4 and T5 temperatures based on NSGA-III and ISOA-BPNN. In steady-state conditions, T4, T5, and exhaust O_2 concentrations increased by 3.14%, 2.07%, and 10.79% on average. NO_x, smoke, and BSFC decreased by 8.68%, 12.07%, and 1.03% on average. In addition, the turbine inlet temperature does not exceed the limit at all operating points, ensuring the efficient and safe regeneration of DPF. This is due to the improvement of fuel injection parameters, thus improving the diesel engine regeneration performance. Building upon the extant optimization methodologies for diesel engine performance, the research effectively refined the regeneration conditions and performance during diesel engine regeneration mode.

(5) Results from regeneration experiments indicate a DPF regeneration efficiency of 88.2%, accompanied by a temperature increase from 711.8°C to 780°C. During the WHTC transient testing, there are significant improvements in T4, T5, and oxygen concentrations, with respective increases of 26%, 3.1%, and 0.5%. In addition, there are notable reductions of 10.4% and 0.8% in NO_x and smoke emissions and a 3.5% decrease in fuel consumption. These results highlight the success of the proposed cyclic optimization method, showcasing improved regeneration under steady-state conditions and significant performance gains under transient conditions.

In future research, further investigations could explore the integration of additional optimization techniques and the development of advanced control strategies to optimize DPF regeneration under varying operating conditions.

Abbreviations

NSGA: Nondominated sorting genetic algorithms
DPF: Diesel particulate filter
BPNN: Backpropagation neural network
BSFC: Brake-specific fuel consumption
T4: DOC inlet temperature
T5: DPF inlet temperature
SOA: Seagull optimization algorithm
ISOA: Improved seagull optimization algorithm
MAPE: Mean absolute percentage error
ECU: Electronic control unit
GA: Genetic algorithm
PSO: Particle swarm optimization
ANN: Artificial neural network
R^2: The correlation coefficient

MAE: Mean absolute error
RMSE: Root mean square error.

Data Availability

The data that support the findings of this study are available from Yunnan Provincial Key Laboratory of Internal Combustion Engines, but restrictions apply to the availability of these data, which were used under license for the current study, and so are not publicly available. However, they are available from the authors upon reasonable request and with permission from Yunnan Provincial Key Laboratory of Internal Combustion Engines.

Conflicts of Interest

The authors declare that they have no conflicts of interest.

Acknowledgments

The research was funded by the Science and Technology Department Unveiling Project of Yunnan Provincial (202104BN050007) Science, Technology Project of Yunnan Province (202102AC080004), and Yunnan Fundamental Research Projects (202401AS070102).

References

[1] X. Duan, Y. Li, J. Liu et al., "Experimental study the effects of various compression ratios and spark timing on performance and emission of a lean-burn heavy-duty spark ignition engine fueled with methane gas and hydrogen blends," *Energy*, vol. 169, pp. 558–571, 2019.

[2] M. J. Eslami, B. Hosseinzadeh Samani, S. Rostami, R. Ebrahimi, and A. Shirneshan, "Investigating and optimizing the mixture of hydrogen-biodiesel and nano-additive on emissions of the engine equipped with exhaust gas recirculation," *Biofuels*, vol. 14, no. 5, pp. 473–484, 2023.

[3] A. Tamilvanan, T. Mohanraj, B. Ashok, and A. Santhoshkumar, "Enhancement of energy conversion and emission reduction of *Calophyllum inophyllum* biodiesel in diesel engine using reactivity controlled compression ignition strategy and TOPSIS optimization," *Energy*, vol. 264, Article ID 126168, 2023.

[4] S. van Dooren, A. Amstutz, and C. H. Onder, "A causal supervisory control strategy for optimal control of a heavy-duty Diesel engine with SCR aftertreatment," *Control Engineering Practice*, vol. 119, Article ID 104982, 2022.

[5] C. McCaffery, J. Yang, G. Karavalakis et al., "Evaluation of small off-road diesel engine emissions and aftertreatment systems," *Energy*, vol. 251, Article ID 123903, 2022.

[6] V. Bermúdez, J. R. Serrano, P. Piqueras, and O. García-Afonso, "Assessment by means of gas dynamic modelling of a pre-turbo diesel particulate filter configuration in a turbocharged HSDI diesel engine under full-load transient operation," *Proceedings of the Institution of Mechanical Engineers-Part D: Journal of Automobile Engineering*, vol. 225, no. 9, pp. 1134–1155, 2011.

[7] Y. Wang, G. Wang, G. Yao, Q. Shen, X. Yu, and S. He, "Combining GA-SVM and NSGA-III multiobjective optimization to reduce the emission and fuel consumption of high-pressure common-rail diesel engine," *Energy*, vol. 278, Article ID 127965, 2023.

[8] S. Rajamohan, M. Thangamuthu, G. K. Pandurangan, S. Vivekanandan, and A. Ramadasan, "Optimization of performance and emission characteristics of compression ignition engine powered with Azolla pinnata fuel blends – a response surface methodology approach," *Energy Sources, Part A: Recovery, Utilization, and Environmental Effects*, pp. 1–10, 2021.

[9] R. Sakthivel, S. Sidharth, P. Ganesh Kumar, T. Mohanraj, A. Tamilvanan, and B. Ashok, *NOx Emission Control Technologies in Stationary and Automotive Internal Combustion Engines*, B. Ashok, Ed., pp. 95–124, Elsevier, Amsterdam, Netherlands, 2022.

[10] H. Taghavifar and F. Mazari, "1D diesel engine cycle modeling integrated with MOPSO optimization for improved NOx control and pressure boost," *Energy*, vol. 247, 2022.

[11] M. Saravanamuthu, R. Thulasiram, D. Ramasamy, and S. Sundaramoorthy, "Optimization of engine parameters using NSGA II for the comprehensive reduction of emissions from VCR engine fuelled with ROME biodiesel," *Environmental Science and Pollution Research International*, vol. 30, no. 22, pp. 61162–61176, 2023.

[12] Q. Zhang, R. M. Ogren, and S. C. Kong, "A comparative study of biodiesel engine performance optimization using enhanced hybrid PSO–GA and basic GA," *Applied Energy*, vol. 165, pp. 676–684, 2016.

[13] H. Bendu, B. Deepak, and S. Murugan, "Multi-objective optimization of ethanol fuelled HCCI engine performance using hybrid GRNN–PSO," *Applied Energy*, vol. 187, pp. 601–611, 2017.

[14] P. K. Bose, M. Deb, R. Banerjee, and A. Majumder, "Multi objective optimization of performance parameters of a single cylinder diesel engine running with hydrogen using a Taguchi-fuzzy based approach," *Energy*, vol. 63, pp. 375–386, 2013.

[15] F. Yang, H. Zhang, S. Song et al., "Thermoeconomic multiobjective optimization of an organic rankine cycle for exhaust waste heat recovery of a diesel engine," *Energy*, vol. 93, 2015.

[16] K. Deb and H. Jain, "An evolutionary many-objective optimization algorithm using reference-point-based nondominated sorting approach, Part I: solving problems with box constraints," *IEEE Transactions on Evolutionary Computation*, vol. 18, no. 4, pp. 577–601, 2014.

[17] H. Jia-Liang, X. Gan, and J. University, *Research on thermal Fault Simulation for marine Diesel Engine Based on BOOST*, Ship Science and Technology, 2015.

[18] B. Garaudee, "Industrial simulation and modeling," *Modeling and Identification of Transient Responses of a Turbo-Charged Diesel Engine for Transfer Function Evaluation*, 1985.

[19] C. Sui, P. de Vos, and D. Stapersma, "Mean value first principle engine model for predicting dynamic behaviour of two-stroke marine diesel engine in various ship propulsion operations- ScienceDirect," *International Journal of Naval Architecture and Ocean Engineering*, vol. 14, 2021.

[20] F. Baldi, G. Theotokatos, and K. Andersson, "Development of a combined mean value–zero dimensional model and application for a large marine four-stroke Diesel engine simulation," *Applied Energy*, vol. 154, pp. 402–415, 2015.

[21] R. Thulasiram, S. Murugan, D. Ramasamy, and S. Sundaramoorthy, "Modelling and evaluation of combustion emission characteristics of COME biodiesel using RSM and ANN—a lead for pollution reduction," *Environmental Science and Pollution Research*, vol. 28, no. 26, pp. 34730–34741, 2021.

[22] J. Zhang, M. R. Amini, I. Kolmanovsky, M. Tsutsumi, and H. Nakada, "Development of a model predictive airpath controller for a diesel engine on a high-fidelity engine model with transient thermal dynamics," in *Proceedings of the 2022 American Control Conference (ACC)*, Atlanta, GA, USA, June 2022.

[23] C. Esonye, O. DominicOfoefule, A. UwaomaOgah, and E. Ogah, "Multi-input multi-output (MIMO) ANN and Nelder-Mead's simplex based modeling of engine performance and combustion emission characteristics of biodiesel-diesel blend in CI diesel engine," *Applied Thermal Engineering: Design, processes, equipment, economics*, vol. 151, 2019.

[24] A. Tamilvanan, K. Balamurugan, T. Mohanraj, and Y. Admassu, "Modeling and optimization of electrodeposition process for copper nanoparticle synthesis using ANN and nature-inspired algorithms," *Journal of Nanomaterials*, vol. 2023, Article ID 3431836, 10 pages, 2023.

[25] P. K. Wong, X. H. Gao, K. I. Wong, and C. M. Vong, "Online extreme learning machine based modeling and optimization for point-by-point engine calibration," *Neurocomputing*, vol. 277, pp. 187–197, 2018.

[26] F. de Nola, G. Giardiello, A. Gimelli, A. Molteni, M. Muccillo, and R. Picariello, "Volumetric efficiency estimation based on neural networks to reduce the experimental effort in engine base calibration," *Fuel*, vol. 244, pp. 31–39, 2019.

[27] A. N. Kumar, P. S. Kishore, K. B. Raju et al., "Decanol proportional effect prediction model as additive in palm biodiesel using ANN and RSM technique for diesel engine," *Energy*, vol. 213, Article ID 119072, 2020.

[28] Ü. Ağbulut, A. E. Gürel, and S. Sarıdemir, "Experimental investigation and prediction of performance and emission responses of a CI engine fuelled with different metal-oxide based nanoparticles–diesel blends using different machine learning algorithms," *Energy*, vol. 215, Article ID 119076, 2021.

[29] M. Aydın, S. Uslu, and M. Bahattin Çelik, "Performance and emission prediction of a compression ignition engine fueled with biodiesel-diesel blends: a combined application of ANN and RSM based optimization," *Fuel*, vol. 269, Article ID 117472, 2020.

[30] X. Zhang, Y. Tian, R. Cheng, and Y. Jin, *IEEE Symposium Series on Computational Intelligence*, IEEE SSCI 2016, Singapore, 2016.

[31] Y. Qian, F. Hou, J. Fan, Q. Lv, X. Fan, and G. Zhang, "Design of a fan-out panel-level SiC MOSFET power module using ant colony optimization-back propagation neural network," *IEEE Transactions on Electron Devices*, vol. 68, no. 7, pp. 3460–3467, 2021.

[32] X. Zhao, D. Xuan, K. Zhao, and Z. Li, "Elman neural network using ant colony optimization algorithm for estimating of state of charge of lithium-ion battery," *Journal of Energy Storage*, vol. 32, Article ID 101789, 2020.

[33] S. Haykin and N. Network, "A comprehensive foundation," *Neural Networks*, vol. 2, 2004.

[34] Y. Kara, M. Acar Boyacioglu, and Ö. K. Baykan, "Predicting direction of stock price index movement using artificial neural networks and support vector machines: the sample of the Istanbul Stock Exchange," *Expert Systems with Applications*, vol. 38, no. 5, pp. 5311–5319, 2011.